[redacted]

NASA TECHNICAL MEMORANDUM

NASA TM X-1042

NASA TM X-1042

[illegible] INVESTIGATION OF THE AERODYNAMICS OF AN APOLLO-SYNC CONFIGURATION AT ANGLES OF ATTACK UP TO 45 DEG. J.J. Jones, et al (NASA) Dec. 1964 35 p

Unclas
00/99 24458

X65 10652
(ACCESSION NUMBER)
35
(PAGES)
(NASA CR OR TMX OR AD NUMBER)
(THRU)
2
(CODE)
01
(CATEGORY)
FACILITY FORM 602

[redacted]

T

By

SHOC
INVE
OF A
AT A

by Jim

Langl

Langl

NATIONAL

CASE FILE COPY

[redacted]

SHOCK-TUNNEL HEAT-TRANSFER INVESTIGATION ON THE AFTERBODY OF AN APOLLO-TYPE CONFIGURATION AT ANGLES OF ATTACK UP TO 45°

By Jim J. Jones and John A. Moore

Langley Research Center
Langley Station, Hampton, Va.

[redacted]

[redacted]

NATIONAL AERONAUTICS AND SPACE ADMINISTRATION

[redacted]

[redacted]

SHOCK-TUNNEL HEAT-TRANSFER INVESTIGATION ON THE AFTERBODY OF AN APOLLO-TYPE CONFIGURATION AT ANGLES OF ATTACK UP TO 45°*

By Jim J. Jones and John A. Moore
Langley Research Center

SUMMARY

10652

A shock-tunnel investigation of the heat transfer to the afterbody of an Apollo-type reentry configuration was made over an angle-of-attack range from 0° to 45°. The stagnation-enthalpy range covered was from 1730 to 8940 Btu/lb, the Mach number varied from 6.5 to 16.1, and the free-stream Reynolds number per foot ranged from 150 to 24000 (Reynolds number based on model diameter ranged from 58 to 6000). The results of the investigation were compared with the results from a wind-tunnel investigation of a similar configuration at a Mach number of 8. (See NASA TM X-813.)

The heat-transfer rates, nondimensionalized by dividing by the stagnation-point heat-transfer rate at 0° angle of attack, were consistently lower than the wind-tunnel data, being about two-thirds the magnitude of the latter. No clearly defined individual variations with Mach number, Reynolds number, or stagnation enthalpy were evident in the data. However, it was shown that for attached boundary layers the Reynolds number effect is the dominant parameter, and the heat transfer was predicted fairly well by use of the reference enthalpy method.

author

INTRODUCTION

A study of the effect of stagnation-enthalpy level on heat-transfer rate is being made by comparing the results of heat-transfer investigations made in a shock tunnel with the results of similar investigations made in the Langley Mach 8 variable-density tunnel. As a part of this program, experiments were made to measure the heat-transfer distribution on the afterbody of an Apollo-type reentry vehicle in both facilities. Since the flow conditions on the afterbody are not well established, particularly at large angle of attack, the configuration is not well suited to a basic study of dissociation effects on heat transfer. However, the immediate need for heat-transfer data on reentry configurations appears to justify the investigation of the configuration.

[redacted]

[redacted]

The results of the investigation in the Mach 8 tunnel at low enthalpy (approximately 350 Btu/lb) were reported in reference 1. The tests in the shock tunnel, reported herein, were conducted over the stagnation-enthalpy range of 1730 to 8940 Btu/lb. (Reservoir temperature ranged from 5630° R to 14130° R.)

SYMBOLS

a	weight fraction of gas which is dissociated
c_p	specific heat at constant pressure, Btu/lb-°R
c_v	specific heat at constant volume, Btu/lb-°R
h	enthalpy, Btu/lb
$\bar{h}/\bar{h}_s$	ratio of heat-transfer coefficient on afterbody to $\alpha = 0°$ stagnation-point heat-transfer coefficient (called h/h_s in ref. 1)
l	length of conical afterbody between tangent points, in.
M_s	shock Mach number
M_∞	test-section Mach number
N_{St}'	Stanton number, $\dfrac{q}{\rho' V_e (h_{aw} - h_w)}$
p	pressure, psia unless otherwise noted
p_r	calculated pressure behind a reflected shock wave in a one-dimensional closed-end shock tube, psia
q	heat-transfer rate to model wall, Btu/ft^2-sec
q_C	stagnation-point heat-transfer rate predicted by theory of Cheng (ref. 2), Btu/ft^2-sec
q_{FR}	stagnation-point heat-transfer rate predicted by theory of Fay and Riddell (ref. 3), Btu/ft^2-sec
R	Reynolds number per foot
R^*	gas constant for undissociated air, 0.0689 Btu/lb-°R
$R_{\bar{x}}'$	Reynolds number based on distance from stagnation point and reference enthalpy method
r/r_{eff}	ratio of model nose radius to effective nose radius (of equivalent sphere)

T	temperature, $^{\circ}R$
V	stream velocity, ft/sec
x	distance along conical afterbody, measured from tangent point, in.
$\bar{x}$	distance along conical afterbody, measured from stagnation point, ft
Z	compressibility factor
α	angle of attack, deg
γ	isentropic exponent
η	recovery factor, $\frac{T_{aw} - T_e}{T_s - T_e}$
ρ	stream density, slugs/ft^3
μ	viscosity, lb-sec/ft^2
ϕ	angle of conical ray, measured from vertical (see fig. 6), deg

Subscripts:

1	conditions in driven tube ahead of incident shock wave
aw	adiabatic wall conditions
D	conditions just downstream of baffle
e	local stream conditions external to boundary layer
f	frozen flow parameters (i.e., vibrational and chemical reactions assumed inactive)
s	stagnation-point conditions behind a normal shock in test section
t	isentropic stagnation conditions
U	conditions just upstream of baffle after shock reflection
w	stream properties evaluated at wall temperature

A prime is used to indicate conditions based on the reference enthalpy method.

TEST FACILITY

A schematic drawing of the shock tunnel is shown in figure 1. The shock tunnel was operated for these tests by using a 76 percent helium, 16 percent hydrogen, and 8 percent oxygen combustion driver and since the tunnel utilized the reflected-shock technique, the stagnation conditions for the nozzle were those behind the reflected normal shock wave. Reference 4 provides a rather complete discussion of shock-tunnel operating techniques. The nozzle is a simple $12\frac{1}{2}^{\circ}$ half-angle conical expansion to a maximum diameter of 3 feet. The geometric area ratio is 5200.

A baffle is installed just ahead of the nozzle minimum section and greatly reduces the number and size of solid particles entering the nozzle. The baffle causes the flow to undergo a short-radius turn (at subsonic speed) which centrifuges most of the heavier particles to the outermost portion of the passage and this portion of the flow is then scooped off and wasted to a dump chamber. The pressure drop across this baffle as measured by quartz piezoelectric transducers located upstream and downstream of it was in most cases less than 10 percent of the upstream value.

Good isolation of the model from the recoil and vibration of the nozzle has been achieved by mounting the model from a platform which rests on a concrete pier that is separate from the tunnel support. The platform is attached to the tunnel only through a rubber pressure seal.

An aluminum diaphragm initially separates the tunnel section, including the baffle section, from the driven tube to permit evacuation of the tunnel test section to a low pressure. This pressure was typically less than 20 microns.

TESTING TECHNIQUE

The shock velocity was determined by plotting the time of arrival of the shock wave at each of ten ionization gaps stationed along the driven tube and graphically determining the local slope of a curve faired through these points. The shock Mach number and corresponding stagnation enthalpy presented with the data are based on the final velocity of the incident shock wave as it approached the end of the driven tube. A correction, which averaged about 5 percent, was made to the stagnation enthalpy as computed for one-dimensional reflected shock to account for an additional compression which occurred as the result of an area change near the nozzle diaphragm. The details of this correction are given in appendix A.

The pressure behind the reflected shock was monitored, as mentioned previously, both upstream and downstream of the baffle. The downstream pressure was taken to be the history of the stagnation pressure of the nozzle, whereas the reading of the upstream pressure transducer immediately after shock reflection was used as a check on the final value of the shock Mach number. (See appendix A.)

The nozzle was surveyed with a pitot-pressure probe using a barium titanate transducer. Sample pressure records of one test run are shown in figure 2 for the upstream and downstream pressures $p_{t,U}$ and $p_{t,D}$, the pitot pressure p_s, and the ratio $p_s/p_{t,D}$, after suitably displacing the time scales to account for the wave transit time through the nozzle. The nozzle Mach number was determined by using the stagnation-pressure ratio $p_s/p_{t,D}$, the computed stagnation enthalpy behind the reflected shock, and the assumption that the flow is in thermal equilibrium throughout the expansion. This last assumption is not necessarily justified for all the test conditions of this program as indicated by several papers on finite reaction rates in nozzles (for example, refs. 5 to 7). The stagnation conditions of the present tests extend from negligible dissociation at the lowest enthalpy to a state in which most of the oxygen is dissociated ahead of the nozzle at the highest enthalpy runs.

The results of a vertical pitot-probe survey of the test section are shown in figure 3 for h_t = 1600 Btu/lb. Surveys at different stagnation-enthalpy levels did not show much effect of enthalpy on test-core size. The stagnation enthalpy does have an important effect on test-section Mach number, however, as shown in figure 4. This figure presents the Mach number, as determined from a pitot probe located near the tunnel center line, plotted against the stagnation enthalpy. Also shown is the one-dimensional calculated variation for a constant-geometry nozzle with an area ratio of 5200. The general trend agrees with the data but the experimental Mach number is high in comparison with the theoretical value.

The experimental stagnation-pressure ratio $p_s/p_{t,D}$ is compared with the value calculated for an area ratio of 5200 as a function of stagnation enthalpy in figure 5. This figure shows that the high experimental values of Mach number presented in figure 4 are the result of a discrepancy of roughly a factor of 2 between experimental total-pressure ratio and calculated values using the geometric area ratio. Inclusion of a correction of the area ratio to account for boundary-layer growth on the nozzle walls would make the agreement poorer. To explain the lack of agreement as the result of the conical flow would appear inconsistent with the vertical-survey results as shown in figure 3. Removal of the baffle assembly caused no appreciable change; thus, the discrepancy would not appear to be due to boundary-layer or wake effects at the nozzle minimum section caused by the baffle. Chemical nonequilibrium would cause some decrease in pitot pressure, but this explanation would not account for the discrepancy at low enthalpy. This anomaly, therefore, has not been resolved at the present time.

During the present tests, a pitot-pressure probe and a stagnation-point heat-transfer probe were mounted in the test section in addition to the heat-transfer model. The pitot-pressure probe served as a check on the steadiness and repeatability of each run. The heat-transfer probe was a 1-inch-diameter sphere with a thick-film heat gage at the stagnation point. It was used to determine the expected heat-transfer rate to the stagnation point of the Apollo model at 0° angle of attack, the quantity by which the afterbody heating rates were divided.

The investigation was begun by using three different shock wave strengths at each angle of attack. The different conditions were achieved by adjusting the initial pressure p_1 to 5, 20, or 100 mm Hg abs. Because the free-stream Reynolds number and heating rates were so low, the initial pressures were doubled to 10, 40, and 200 mm Hg abs. The driver pressure and diaphragm strength were also doubled, so that approximately the same shock Mach numbers were achieved. This increase in driver pressure resulted in occasional detonations during combustion, which caused the loss of some test runs as well as the time necessary to repair any resulting damage, but the higher Reynolds number and increased heat-transfer rates appeared to warrant the effort.

MODELS AND DATA REDUCTION TECHNIQUE

A sketch of the model configuration is presented in figure 6. Each model was constructed of steel with a pyrex insert making up half of the conical afterbody. Five thin-film platinum-resistance thermometers similar to those elements used in reference 8 were applied to each model with low-resistance silver paint used as leads to a convenient location to attach wires. Figure 7 is a photograph of one of the models tested. The models were contributed by Republic Aviation Corp.

Five models were tested in the present program. Two were axial-distribution models (designated models 2 and 4) on which the thermometer elements were arranged along the $\phi = 0^{\circ}$ ray, which became the most windward ray at angle of attack. The other three models (1, 3, and 5) were lateral-distribution models with all five thermometer elements of each model at the same x station and spaced at 30° increments from $\phi = -60^{\circ}$ to 60°. Figure 6 indicates the location of the center of each thermometer element on all five models. Each thermometer element, because of its finite size, actually averaged the surface temperature over an axial length of one-sixteenth of an inch and a lateral angle ranging from 8° for the most forward element to about 16° for the most rearward element.

Two different struts were used to cover the angle-of-attack range of 0° to 45°. For low angles of attack the strut met the conical afterbody normal to its surface and thus the acute angle between the center line of the strut and the axis of the model was 55° (see fig. 6). For high angles of attack a different strut was used in which the strut center line was normal to the axis of the model. Thus, these struts were similar to sting 1 and sting 2 used in the investigation of reference 1.

The oscilloscope records of temperature-time histories were read and programed into a computer for computation of heat-transfer rate q. The heat-transfer rate was computed at 0.5-millisecond intervals for a period of about 6 milliseconds on most runs. The method used for reducing temperature-time records to heat-transfer rate is outlined in reference 8. An example of the variation of heat-transfer rate with time is shown in figure 8. The rate at 0.5 millisecond was frequently scattered due to the starting process in the nozzle (zero time was taken to be the instant when the shock wave passed by the

model). Disregarding this first data point, the heat-transfer rate was averaged over the time interval from 1 millisecond to 3 milliseconds and this average is the value presented. The stagnation-point heating rate was also averaged over the same time interval. This average was then adjusted to the value expected on the model stagnation point at $\alpha = 0^{\circ}$ by multiplying by $\sqrt{r/r_{eff}}$ where r_{eff}, the effective nose radius of the Apollo configuration, was calculated by the method of reference 9 and found to be equal to the maximum body diameter. Figure 8 illustrates the fact that, although the heat-transfer rate varied with time on many runs, dividing by the stagnation-point heat-transfer rate q_s gave a result that was more constant with time. The sphere heating rate is compared with that predicted by theory in appendix A.

RESULTS AND DISCUSSION

All the data of this test program are presented in table I. The results of the runs on the two axial-distribution models are presented in figure 9. Also shown in the figure are the low Reynolds number data of reference 1, for angles of attack of 0°, 25°, 35°, and 45°. The Mach 8 tunnel data of reference 1 are presented in heat-transfer-coefficient form $\bar{h}/\bar{h}_s$ (called h/h_s in ref. 1), whereas the present data were left in the form of heat-transfer rate q/q_s because of the uncertainties in evaluating the adiabatic-wall temperature on the afterbody. The two forms are related by

$$\frac{\bar{h}}{\bar{h}_s} = \frac{q}{q_s}\,\frac{T_s - T_w}{T_{aw} - T_w}$$

Introducing the recovery factor η and rearranging gives the relation

$$\frac{\bar{h}}{\bar{h}_s} = \frac{q}{q_s}\left[1 - (1 - \eta)\frac{1 - \frac{T_e}{T_s}}{1 - \frac{T_w}{T_s}}\right]^{-1}$$

where T_e is the local stream temperature external to the boundary layer. For those cases where the boundary layer is attached, the present data may, with certain assumptions, be converted to heat-transfer-coefficient ratio. If an attached laminar boundary layer is assumed ($\eta = 0.85$) and if $\left(1 - \frac{T_w}{T_s}\right) = 0.9$ is used (since T_w/T_s for the present tests varies from 0.058 to 0.116), the relation becomes

$$\frac{\bar{h}}{\bar{h}_s} = \frac{q}{q_s}\,\frac{0.9}{0.9 - 0.15\left(1 - \frac{T_e}{T_s}\right)}$$

Calculation indicates that values of T_e/T_s range from about 1/3 to 2/3 for the present data, depending on stagnation enthalpy, angle of attack, and

assumption as to gas state. Thus the correction would be about 6 to 12 percent. Figure 9 shows that this correction would not appreciably change the relation of the present data to the Mach 8 tunnel data.

The data at $\alpha = 0^{\circ}$ are scattered between $q/q_s = 0.01$ and 0.03. The Mach 8 tunnel data also showed considerable scatter at $\alpha = 0^{\circ}$, and were shown to be subject to sting interference effects, particularly near the rear of the afterbody. In spite of the scatter, however, it appears clear that the present shock-tunnel data tend to be lower than the Mach 8 tunnel data at low angles of attack, averaging perhaps two-thirds of the latter. At higher angle of attack, however, the data approach one another and are in essential agreement at $\alpha = 45^{\circ}$.

Figure 9 shows that in both the present data and those of reference 1, very little tendency of heat-transfer ratio to change with distance x/l is observed at low angles of attack. At the higher angles of attack, both sets of data show a trend toward decreasing heat-transfer ratio with increasing distance. The onset of this trend is assumed to be the result of flow attachment on the afterbody. This assumption results in the conclusion that flow attachment occurs at lower angle of attack for the present shock-tunnel data than for the Mach 8 tunnel data. At $\alpha = 25^{\circ}$ the trend is definitely apparent in the present data, indicating flow attachment, whereas the reference 1 data appear to be separated.

The data obtained from the lateral-distribution models are presented in figure 10. It may be seen that for many of the runs, particularly on model 1, the distribution is not symmetrical about the $\phi = 0^{\circ}$ ray; the data at $\phi = 30^{\circ}$ show a tendency to be higher than that at $\phi = -30^{\circ}$. An effort was made to determine if this was due to flow angularity. A wedge was mounted in the test section at the same location at which the heat-transfer models had been, with its leading edge vertical and normal to the tunnel center line. A pressure transducer was mounted in each face of the wedge and the pressures measured by these transducers were compared. Within the accuracy of the measurement, the transducers indicated that the wedge was at 0° angle of yaw. It was concluded that the asymmetry was not due to flow angularity. The possibility exists that this asymmetry is due to a disturbance at the metal-to-glass joint upstream of the heat-transfer elements. This joint appeared to be quite fair and smooth on all models, but the boundary layer is very thin around the rim and small disturbances might be expected to produce magnified effects for some distance downstream. Since model 1 had its thermometer elements closer to this joint than the other models, it might be expected to be more sensitive to the quality of the joint.

Essentially three pertinent flow parameters were varied in the present tests: Mach number, Reynolds number, and stagnation enthalpy. Because the shock tunnel was operated at fixed area-ratio and driver conditions, the parameters are interdependent; that is, no single parameter was varied independently of the others. Specifically, the data show a trend toward lower heat-transfer ratio (q/q_s) as the stagnation enthalpy is increased, but the increase in enthalpy is accompanied by a decrease in Reynolds number and Mach number so that it is impossible to assess the individual effects of each parameter.

At high angles of attack where the boundary layer is attached, the rapid decrease in heat transfer with increasing axial distance noted for the present data and the reference 1 data suggests a comparison with flat-plate predictions. Furthermore, there is a trend toward lower heat-transfer ratio for lower unit Reynolds number in both sets of data. It would be interesting to see to what extent this Reynolds number trend in the wind-tunnel data, where no dissociation was present, would account for the heat rate in the shock-tunnel data. For this purpose the data along the $\phi = 0^{\circ}$ ray at $\alpha = 35^{\circ}$ were reduced to Stanton number and Reynolds number and are presented in figure 11. In order to reduce the shock-tunnel data to this form, it was necessary to make a number of assumptions to permit calculation of local flow conditions. Since no pressure-distribution data were obtained in the present tests, the pressure distribution p/p_s as a function of x/l obtained in reference 1 was assumed to apply. The expansion from equilibrium stagnation conditions was assumed to be completely frozen with regard to vibrational and chemical reactions. In order to compare the data with the incompressible flat-plate prediction, the reference-enthalpy method of reference 10 was used to evaluate the temperature at which ρ' and μ' were determined. The details are covered in appendix B.

Figure 11 shows the correlation of the present data along the $\phi = 0^{\circ}$ ray at $\alpha = 35^{\circ}$ reduced in the manner described, as well as the data of reference 1, with the incompressible flat-plate prediction using the modified Reynolds analogy. (Prandtl number was taken to be 0.71.) Fair agreement is shown with flat-plate theory even though the flow over the model differs considerably from flat-plate flow. A large favorable pressure gradient is encountered by the flow as it expands around the rim but this is confined to a region near the stagnation point (leading edge) and the pressure gradient along the conical portion of the afterbody is not large; therefore, the overall effect of the pressure gradient may be small. The boundary-layer thinning effect of the cross flow is opposed by the thickening effect of the converging wetted area of the surface.

Figure 11 shows that the Mach 8 wind-tunnel data and the present shock-tunnel data both lie a little below the flat-plate prediction but the slope of the line predicts the Reynolds number effect quite well. Different symbols were used for the present data in figure 11 according to the stagnation-enthalpy range in which they fell in order to see if a definite effect of stagnation enthalpy was apparent. There appears to be a slight trend toward lower heating with increasing enthalpy at a given Reynolds number, but the trend is inconclusive owing to the scatter of the data.

CONCLUDING REMARKS

In the present investigation, measurements of the heat-transfer rate to the afterbody of an Apollo-type configuration were made in a shock tunnel and the results compared with those of a similar investigation made in a conventional Mach 8 wind tunnel (NASA TM X-813). The present investigation extended over a stagnation-enthalpy range from 1730 to 8940 Btu/lb. The Mach number varied from 6.5 to 16.1 and the free-stream Reynolds number per foot ranged from 150 to 24000.

Except for the highest angle of attack the nondimensionalized heating rates obtained in the present investigation were lower than those obtained in the Mach 8 tunnel investigation. This result is consistent with the trend of the wind-tunnel data, which shows lower heating rates at the lower Reynolds numbers. For the present data it was not possible to determine any trends which could be attributed to Mach number, Reynolds number, or stagnation enthalpy, either because these trends are slight or tended to compensate each other in the present program. However, it was shown that for an angle of attack of 35°, where the boundary layer was attached along the most windward ray, the present shock-tunnel data can be correlated fairly well with the wind-tunnel data when reduced to Stanton number and Reynolds number based on reference enthalpy conditions.

Langley Research Center,
National Aeronautics and Space Administration,
Langley Station, Hampton, Va., September 11, 1964.

APPENDIX A

COMPARISON OF MEASURED STAGNATION PRESSURE AND STAGNATION-POINT HEAT-TRANSFER RATE TO CALCULATED VALUES

The data from the shock tunnel have indicated the measured pressure behind the reflected shock wave immediately after shock reflection to be somewhat low in comparison with the computed pressure using the measured values of initial pressure p_1 and the final value of shock Mach number M_s. Examination of the differences between actual tube geometry and the assumed ideal condition of a constant-area closed-end tube has disclosed much of the discrepancy.

The accompanying sketch shows approximately the geometry and one-dimensional area distribution at the diaphragm and baffle location. An area increase occurs at the end of the low-pressure tube extending to about 3 inches upstream of the diaphragm, as a result of a telescoping section which facilitates changing the nozzle diaphragm. This increase in internal diameter amounts to a 25-percent increase in area. Thus the shock wave immediately after reflection is traveling into gas at somewhat different conditions than in the constant-area portion of the tube.

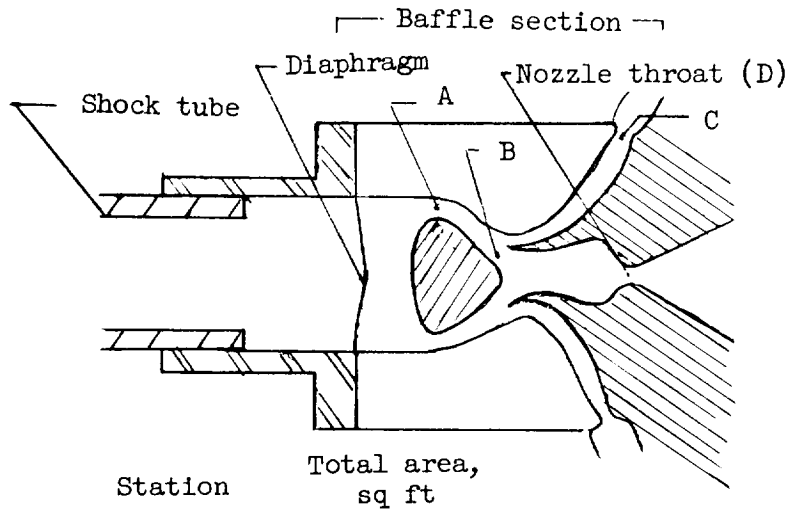

Station	Total area, sq ft
A	0.0078
B	.0079
C	.0028
D	.0014

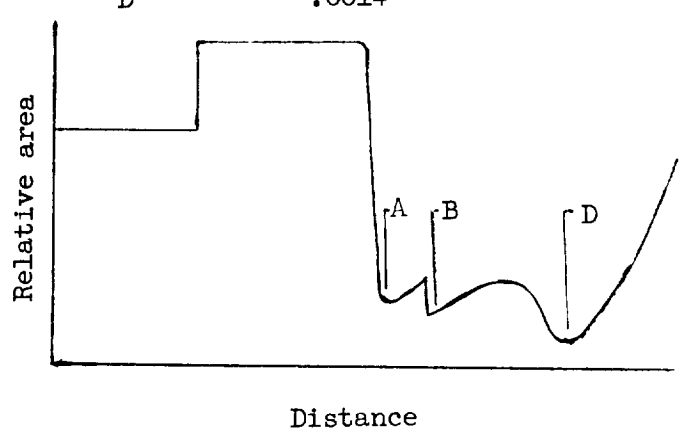

For purposes of calculation, the gas was assumed to expand isentropically to a new area equal to 1.25 times the initial area and this expanded condition was then the state of the gas into which the reflected shock traveled. When the shock wave has advanced up to the location of the area change, the conditions behind the shock will of course be perturbed.

Instead of using the boundary condition of zero velocity behind the reflected shock wave, a finite velocity was assumed which accounted for the flow

into the baffle section. This velocity was calculated with the assumption that the minimum area of the baffle passage (area A on sketch) was choked, a condition that would exist only for a short time, approximately 200μ sec, since this baffle minimum area was five times greater than the nozzle throat area.

The critical areas of the baffle assembly are indicated in the sketch. The total area of the exit passages of the baffle (the throat area at station D plus the bypass area at station C) is equal to 0.54 times the minimum area of the baffle at station A. Thus when steady flow is established and the baffle exits at stations C and D are choked, the Mach number at station A would be about 0.3.

Stagnation-pressure calculations were made of the configuration just described. These calculations covered the range of incident shock Mach numbers of the present investigation and the resulting pressures were compared with p_r, the calculated value for a constant-area closed-end case. It was found that the ratio of these pressures was essentially constant, the pressure of the more exact case being 0.77 times p_r. The comparison of this result with the experimental data is made in figure 12, where the experimental pressure measured behind the reflected shock $p_{t,U}$ is plotted against the calculated reflected pressure p_r by using the measured values of shock Mach number and initial pressure and assuming constant area and no outflow. The solid line in figure 12 is the 1:1 correlation representing the constant-area reflected-shock pressure; the dashed line is equal to 0.77 times this calculated pressure and thus represents the described stepped-area distribution with outflow for areas C and D choked. The scatter of the data is rather large but it may be seen that the $0.77p_r$ line is a reasonable approximation to the data, particularly for the higher pressure conditions. One reason for the scatter is an accuracy problem; it is necessary to read the pressure record immediately after shock reflection where the amplitude of oscillation of the pressure record is greatest, and only 3 or 4 cycles of the oscillation are completed before the pressure changes because of the shock reentering the smaller area tubing.

The stagnation enthalpy is affected much less than the pressure by geometry considerations. In all calculated cases the geometry change caused less than a 2-percent change in stagnation enthalpy immediately after shock reflection. However, when the reflected shock has traveled through the telescoping section and reenters the smaller diameter tube, the gas state is perturbed, and the pressure transducer indicated that the pressure rises to approximately the value expected behind a one-dimensional reflected shock in a constant-area tube. This additional compression was treated as isentropic for the purpose of determining the new enthalpy, and this final value of the stagnation enthalpy is the value used in determining the free-stream conditions and is given in table I. The resulting enthalpy increase was, in most cases, about 5 percent.

Because of the low Reynolds numbers of the tests, it was anticipated that the stagnation-point heat-transfer rate might be predicted more accurately by a shock-layer analysis such as that of Cheng in reference 2 rather than by an inviscid-boundary-layer approach. Figure 13 presents the stagnation-point heat-transfer rate obtained on the sphere for each of the runs of the present investigation. In figure 13(a), the sphere heating rate q_s is divided by q_{FR},

the heat-transfer rate that would be predicted by the analysis of Fay and Riddell in reference 3. In figure 13(b), q_s is divided by q_C, the heat-transfer rate predicted by the analysis of Cheng in reference 2. At low shock Mach number, the present data q_s show better agreement with q_C, the shock-layer analysis which accounts for the viscous and heat-conduction effects immediately behind the bow shock wave. The scatter in the data reflects not only the accuracy of determining heat-transfer rate but also the determination of local stream conditions.

APPENDIX B

REDUCTION OF THE PRESENT DATA TO STANTON NUMBERS AND REYNOLDS NUMBERS BASED ON REFERENCE ENTHALPY

In order to obtain local flow conditions for the present data, it was necessary to make a number of assumptions, since only heat-transfer rate was measured on the afterbody. The experimental pressure distribution p/p_s as a function of x/l obtained in reference 1 was assumed to apply to the present tests. The stagnation-point location at $\alpha = 35^{\circ}$ was also assumed to be the same. Since the density was so low in the shock-tunnel tests, it was believed that the assumption of frozen flow (vibrational and chemical reaction rates equal to zero) in the expansion around the body from the stagnation point is a good approximation of the actual conditions.

Local stream properties were calculated by using isentropic relations and assuming a "frozen" value for the ratio of specific heats as the isentropic exponent. For a partly dissociated gas whose only active degrees of freedom are translation and rotation, the ratio of specific heats can be expressed in a simple form. First, the specific heat at constant volume can be expressed as

$$(c_v)_f = a\,\frac{3}{2}\,2R^* + (1 - a)\frac{5}{2}\,R^*$$

where a is the weight fraction of the gas which is dissociated; thus, $a = Z - 1$. This equation assumes that the gas constant for the atomic fraction is just twice that for the diatomic fraction. The specific-heat ratio can then be written as

$$\gamma_f = \left(\frac{c_p}{c_v}\right)_f = 1 + \frac{ZR^*}{(c_v)_f}$$

or

$$\gamma_f = \frac{7 + 3a}{5 + a}$$

By utilizing this result as the isentropic exponent in ideal-gas relations and by starting with the equilibrium state at the stagnation point, the local inviscid flow conditions on the afterbody may be expressed as follows:

$$\frac{\rho_e}{\rho_s} = \left(\frac{p_e}{p_s}\right)^{1/\gamma_f}$$

$$\frac{T_e}{T_s} = \left(\frac{p_e}{p_s}\right)^{(\gamma_f-1)/\gamma_f}$$

$$h_s - h_e = (c_p)_f(T_s - T_e)$$

If a recovery factor $\eta = 0.85$ is assumed, the adiabatic-wall enthalpy is given by

$$h_{aw} = h_e + 0.85(h_s - h_e)$$

The reference enthalpy is determined from

$$h' = h_e + 0.5(h_w - h_e) + 0.22(h_{aw} - h_e)$$

and the density and viscosity are then evaluated at T' and p_e, where T' is found from a Mollier diagram for equilibrium air (ref. 11) at h' and p_e.

Stanton number and Reynolds number are then defined as

$$N_{St}' = \frac{q}{\rho' V_e(h_{aw} - h_w)}$$

$$R_{\bar{x}}' = \frac{\rho' V_e \bar{x}}{\mu'}$$

where $\bar{x}$ is measured from the stagnation point. The stagnation-point location was determined from reference 1.

Note that the use of a Mollier diagram to find T' assumes that chemical and vibrational equilibria are reached in the boundary layer and that the energy which was frozen in the free stream is included as part of the driving enthalpy potential in calculating Stanton number.

REFERENCES

1. Jones, Robert A.: Experimental Investigation of the Overall Pressure Distribution, Flow Field, and Afterbody Heat-Transfer Distribution of an Apollo Reentry Configuration at a Mach Number of 8. NASA TM X-813, 1963. (Supersedes NASA TM X-699.)

2. Cheng, Hsien K.: Hypersonic Shock-Layer Theory of the Stagnation Region at Low Reynolds Number. Rep. No. AF-1285-A-7 (Contract Nonr-2653(00)), Cornell Aero. Lab., Inc., Apr. 1961. (Available from ASTIA as AD 256 745.)

3. Fay, J. A.; and Riddell, F. R.: Theory of Stagnation Point Heat Transfer in Dissociated Air. Jour. Aero. Sci., vol. 25, no. 2, Feb. 1958, pp. 73-85, 121.

4. Hertzberg, A.; Wittliff, Charles E.; and Hall, J. Gordon: Summary of Shock Tunnel Development and Application to Hypersonic Research. Rep. No. AD-1052-A-12 (Contract AF 18(603)-10), Cornell Aero. Lab., Inc., July 1961.

5. Hall, J. Gordon; and Russo, Anthony L.: Studies of Chemical Nonequilibrium in Hypersonic Nozzle Flows. Rep. No. AD-1118-A-6 (Contract AF 18(603-141), Cornell Aero. Lab., Inc., Nov. 1959.

6. Eschenroeder, Alan Q.; Boyer, Donald W.; and Hall, J. Gordon: Nonequilibrium Expansions of Air With Coupled Chemical Reactions. The Phys. of Fluids, vol. 5, no. 5, May 1962, pp. 615-624.

7. Nagamatsu, H. T.; Workman, J. B.; and Sheer, R. E., Jr.: Hypersonic Nozzle Expansion of Air With Atom Recombination Present. Jour. Aerospace Sci., vol. 28, no. 11, Nov. 1961, pp. 833-837.

8. Jones, Jim J.: Shock-Tube Heat-Transfer Measurements on Inner Surface of a Cylinder (Simulating a Flat Plate) for Stagnation-Temperature Range 4,100° to 8,300° R. NASA TN D-54, 1959.

9. Boison, J. Christopher; and Curtiss, Howard A.: An Experimental Investigation of Blunt Body Stagnation Point Velocity Gradient. ARS Jour., vol. 29, no. 2, Feb. 1959, pp. 130-135.

10. Eckert, Ernst R. G.: Survey on Heat Transfer at High Speeds. WADC Tech. Rep. 54-70, U.S. Air Force, Apr. 1954.

11. Moeckel, W. E.; and Weston, Kenneth C.: Composition and Thermodynamic Properties of Air in Chemical Equilibrium. NACA TN 4265, 1958.

[redacted]

TABLE I.- MEASURED HEAT-TRANSFER RATES AND TEST CONDITIONS

Run	Model	α, deg	p, mm Hg abs	M_s	h_t, Btu/lb	R, 1/ft	M_∞	q_s, Btu/ft^2-sec	q, Btu/ft^2-sec, at afterbody thermometer element -				
									1	2	3	4	5
1507	2	20	19.9	8.0	3700	1490	12.2	27.0	1.0	-----	-----	0.75	0.8
1508	2	20	4.7	9.6	5750	447	9.5	24.7	1.0	1.0	0.75	.75	.8
1510	2	20	100	6.1	2140	8680	15.6	19.35	1.2	1.1	.8	.65	.7
1511	2	20	100	6.3	2270	9900	15.3	23.8	-----	1.3	1.1	.7	.85
1512	2	10	20	8.6	4110	-----	-----	39.5	.7	-----	.7	-----	.8
1513	2	10	99	6.25	2180	10200	15.6	22.0	.45	-----	.45	.7	.7
1514	2	10	4.85	11.5	7750	381	7.3	39.5	.6	-----	.9	.7	.8
1515	1	20	20	8.8	4535	1370	11.0	33.8	.7	-----	1.25	-----	1.0
1538	1	20	100	6.0	2180	9400	15.2	16.7	.65	.5	1.75	1.25	.75
1540	1	20	20	9.1	4600	1390	10.7	22.7	.6	.6	1.3	1.3	1.0
1541	1	20	4.8	10.2	6300	481	8.6	23.0	1.0	.65	1.25	1.25	1.2
1542	1	30	4.9	10.8	6570	332	8.3	20.7	1.2	.55	1.3	1.3	1.0
1544	1	30	19.9	8.4	4030	1870	11.7	26.3	1.15	1.0	2.0	1.9	1.5
1545	1	30	100.5	6.0	2010	12770	15.8	16.1	1.0	.9	1.6	1.75	1.1
1546	1	35	101	6.4	2310	9900	15.4	18.7	1.5	1.25	2.0	2.4	1.2
1547	1	35	20	8.0	3720	1720	12.5	19.5	1.5	1.0	2.0	2.0	1.0
1548	1	35	5.0	12.0	8060	214	7.25	25.5	-----	.8	1.9	2.25	----
1549	1	35	5.0	10.4	6600	389	8.4	29.5	1.5	1.3	2.5	2.75	----
1550	1	35	200	5.4	1740	21100	16.1	17.5	-----	1.25	1.65	1.75	1.25
1551	1	45	5.0	10.4	6330	317	8.6	20.3	.5	1.2	2.75	2.75	1.2
1552	1	45	20	9.6	4910	566	10.3	11.5	1.0	.75	2.3	2.4	1.25
1553	1	45	19.9	7.4	3110	1760	13.3	13.1	1.5	1.4	2.25	2.0	.8
1554	1	45	20	7.4	3120	1330	13.5	11.5	1.0	1.2	2.1	2.1	.6
1556	1	45	100	5.5	1730	12000	16.0	10.0	.5	1.25	2.0	2.0	1.2
1562	4	0	100	5.6	1920	12000	15.6	14.7	.25	.25	.25	.25	.25
1563	4	25	5	9.9	6110	460	8.9	33.2	-----	1.5	1.15	1.15	.9
1564	4	25	20	8.4	4110	1690	11.8	29.8	2.3	1.8	1.4	-----	----
1566	4	25	40	8.0	3830	3860	12.3	46.2	3.6	2.8	2.2	1.6	1.25
1570	4	35	40	7.2	3480	4880	13.1	33.0	5.9	5.0	4.0	2.55	2.15
1571	4	35	200	5.4	1725	23400	15.6	16.1	2.2	1.65	1.75	1.0	.85
1572	4	35	10	9.8	6170	1680	9.2	51.8	7.1	4.5	4.5	3.0	2.5
1573	4	45	40	8.1	4040	2480	12.2	31.0	10	8.5	7.2	4.5	3.5
1574	4	45	10	10.0	5620	820	9.8	39.3	9	8.5	7	4.6	3
1578	4	45	200	7.1	2800	13500	14.3	36.6	19	14	11.2	10	9.2
1579	3	20	40	8.5	4360	2390	11.65	42.0	-----	1.92	2.4	2.25	1.65
1580	3	20	10	11.15	7600	410	7.6	39.2	2.65	2.4	2.5	2.1	2.0
1581	3	20	200	6.2	2720	11800	14.0	30.3	1.5	1.75	2.1	2.1	1.20
1582	3	30	40	9.6	5100	1300	10.8	34.7	2.3	2.6	3.35	4.25	2.1
1583	3	30	10	12.8	8700	470	7.1	50.6	3.0	3.8	4.65	5.4	2.85
1584	3	30	200	5.8	2020	18000	16.0	21.9	1.5	1.8	2.55	2.1	1.6
1586	3	35	40	8.1	3830	2760	12.4	32.9	2.65	3.0	4.15	4.7	2.35
1587	3	35	10	10.0	5900	1020	9.0	40.3	3.25	3.75	5.4	4.75	2.95
1588	3	35	200	6.1	2200	21200	15.0	30.2	2.8	3.15	4.3	3.9	2.45
1589	3	45	39.5	8.0	3550	4600	12.6	33.1	3.8	5	9.3	10	3.1
1591	3	45	200	6.0	2370	20300	14.0	26.3	3.5	4.2	10	5.2	2.9
1592	5	20	40	8.2	3730	2850	12.3	36.8	1.2	1.15	-----	.98	.90
1593	5	20	10.2	12.6	8940	760	6.5	45.3	1.3	1.25	1.55	.9	.5
1594	5	20	200	6.8	2560	17500	14.0	32.3	1.05	1.1	1.5	-----	----
1595	5	30	40	8.3	4130	3700	11.3	36.3	1.3	1.55	2.2	1.85	1.1
1596	5	30	10	10.7	6780	724	8.7	39.4	1.45	1.65	2.2	2	1.15
1597	5	30	200	6.7	2500	13100	14.2	27.9	1.3	1.3	1.85	1.15	1.0
1598	5	35	39	8.7	4490	3540	10.7	40.2	1.55	1.75	2.65	1.8	1.3
1599	5	35	10	9.2	5640	1075	9.0	39.2	1.35	1.7	2.3	1.25	.85
1600	5	35	200	6.0	2140	23700	14.6	28.0	1.3	1.8	2.35	1.85	1.2
1604	5	45	10	11.6	7570	368	7.8	39.7	1.9	3.3	8.2	3.4	1.3
1605	5	45	40	8.3	4470	2450	11.35	36.0	1.9	3.0	4.7	3.4	1.6
1606	5	45	200	6.1	2230	20400	15.0	29.3	1.4	3.0	7.0	1.8	1.3
1609	2	0	200	6.0	2130	22000	14.9	27.3	.56	.46	.56	.32	.52
1612	2	0	40	8.0	3800	4300	11.5	27.7	-----	.60	.72	.42	.87
1613	2	0	200	6.0	2100	22000	14.9	27.7	.44	.44	.53	.24	.52

[redacted]

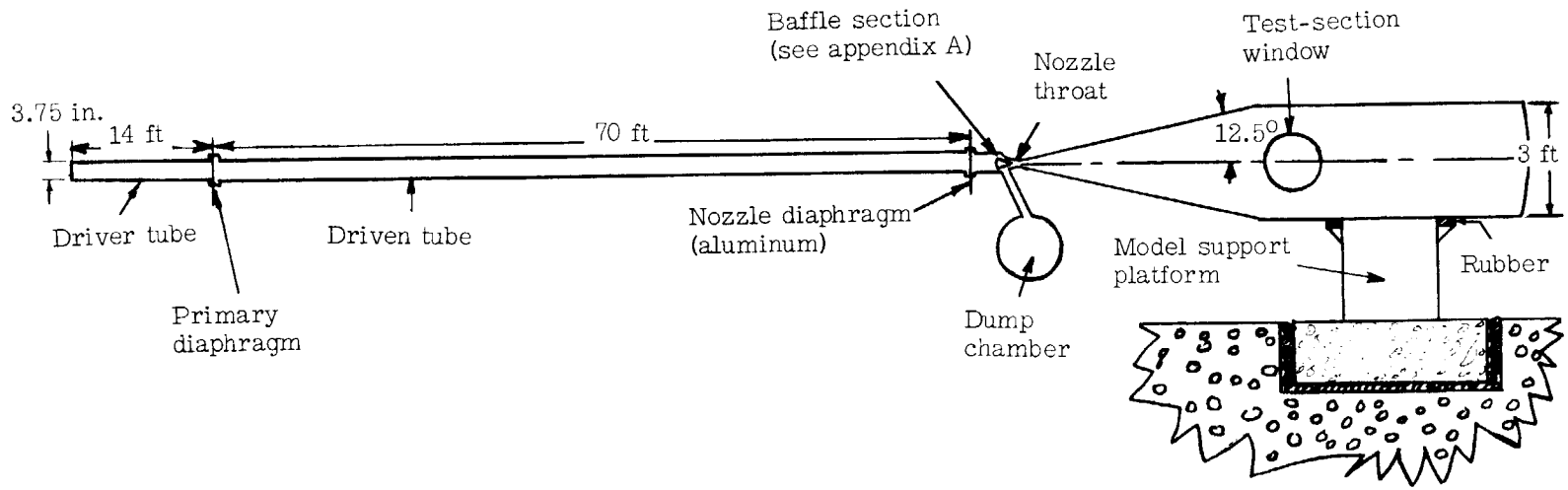

Figure 1.- Schematic drawing of shock tunnel.

[redacted]

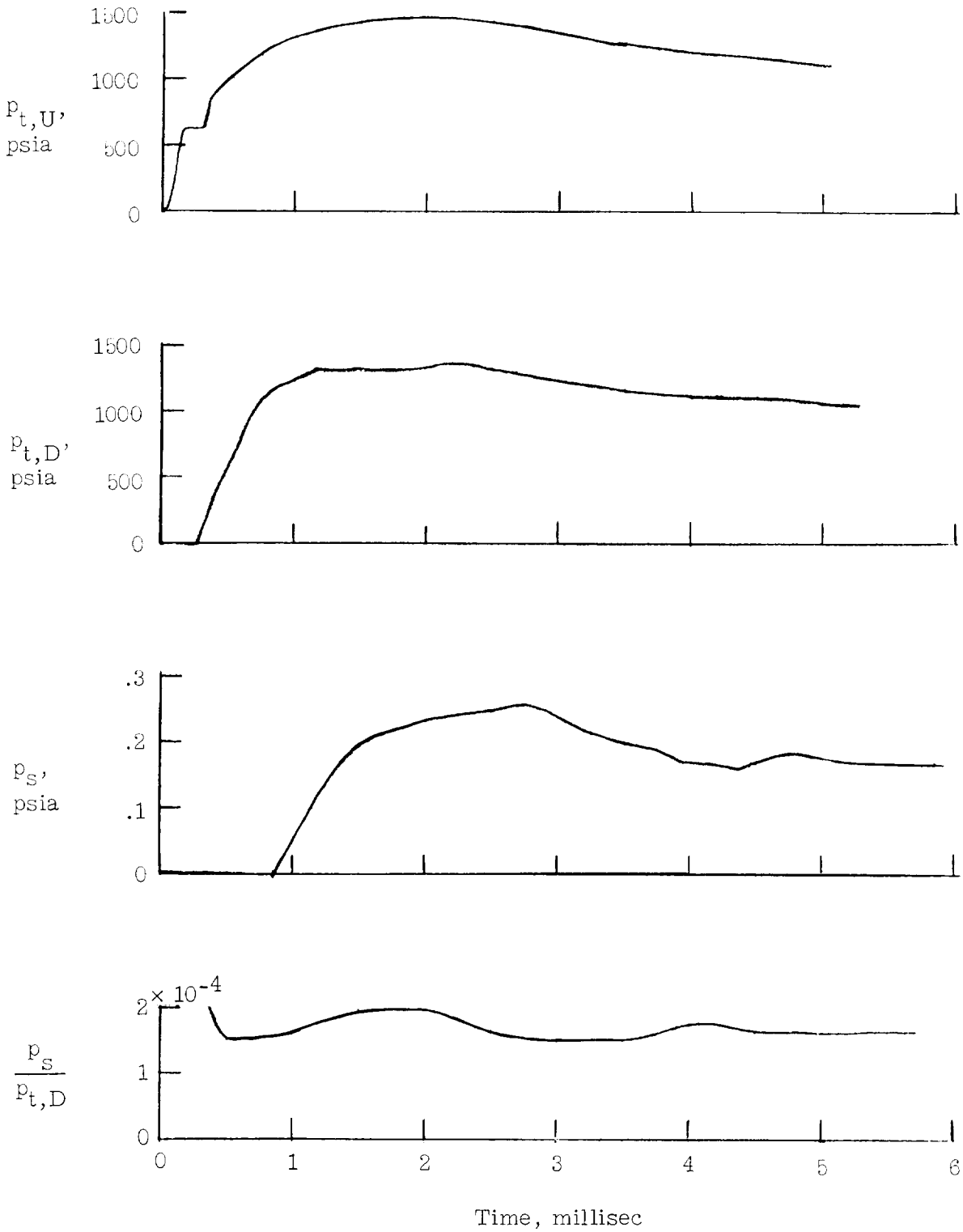

Figure 2.- Sample pressure records of one run (run 1606).

[redacted]

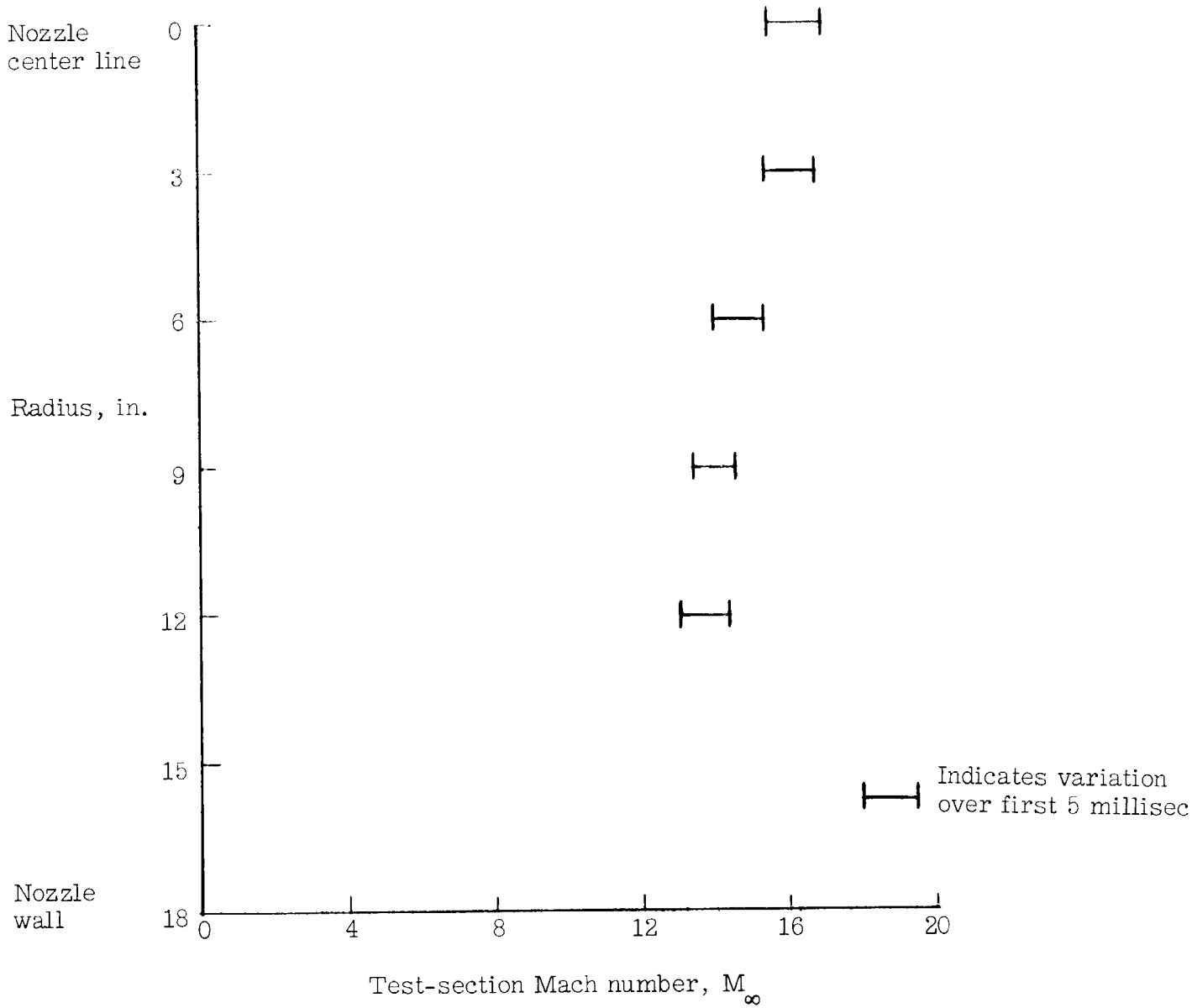

Figure 3.- Results of vertical pitot-probe survey. $h_t \approx 1600$ Btu/lb.

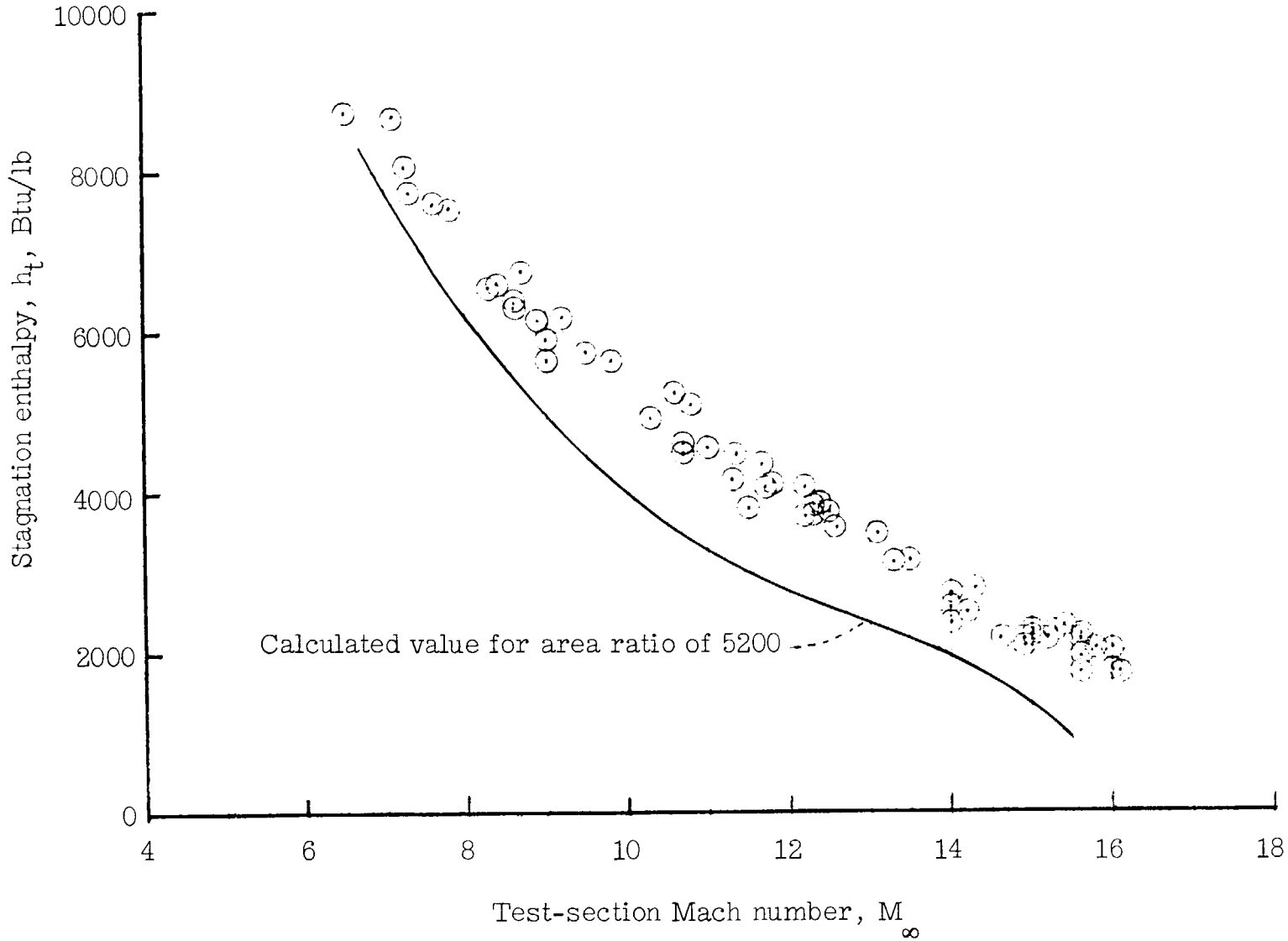

Figure 4.- Variation of test-section Mach number with stagnation enthalpy.

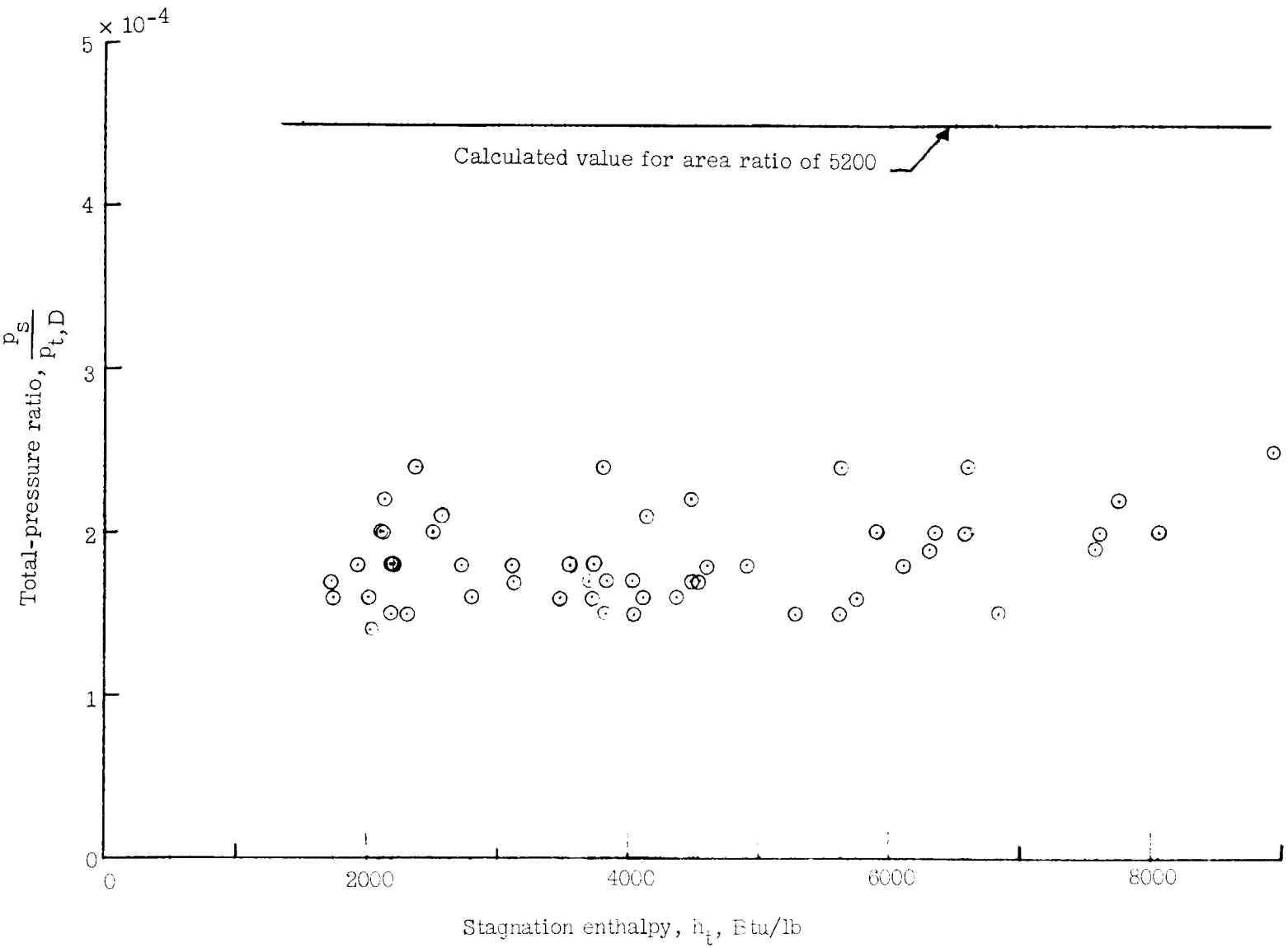

Figure 5.- Experimental total-pressure ratio as a function of stagnation enthalpy.

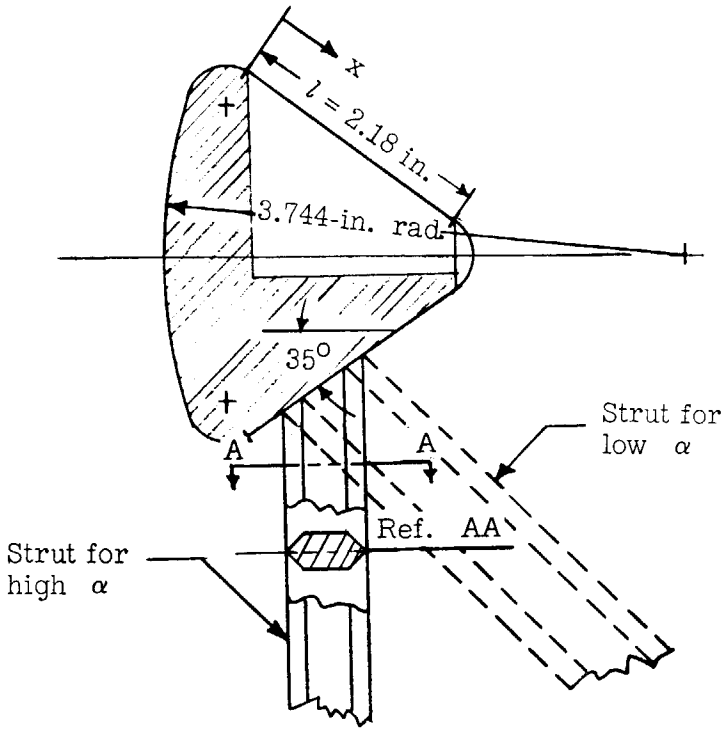

LATERAL-DISTRIBUTION MODELS

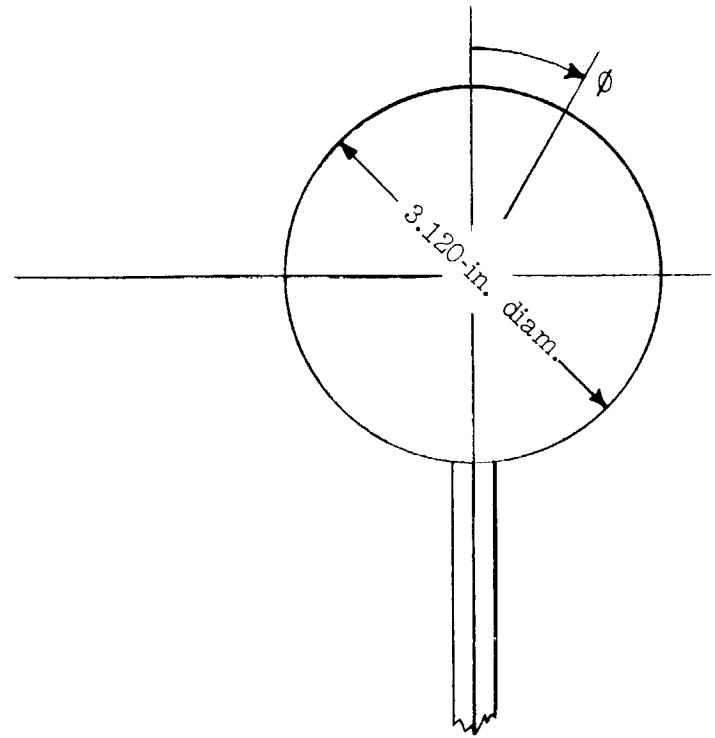

AXIAL-DISTRIBUTION MODELS

Model	x, in.	ø, deg, for thermometer element -				
		1	2	3	4	5
1	0.25	-60	-30	0	30	60
3	.50	-60	-30	0	30	60
5	1.50	-60	-30	0	30	60

Model	ø, deg	x, in., for thermometer element -				
		1	2	3	4	5
2	0	0.375	0.750	1.125	1.50	1.875
4	0	.125	.500	.905	1.28	1.625

Figure 6.- Sketch of model configuration.

[redacted]

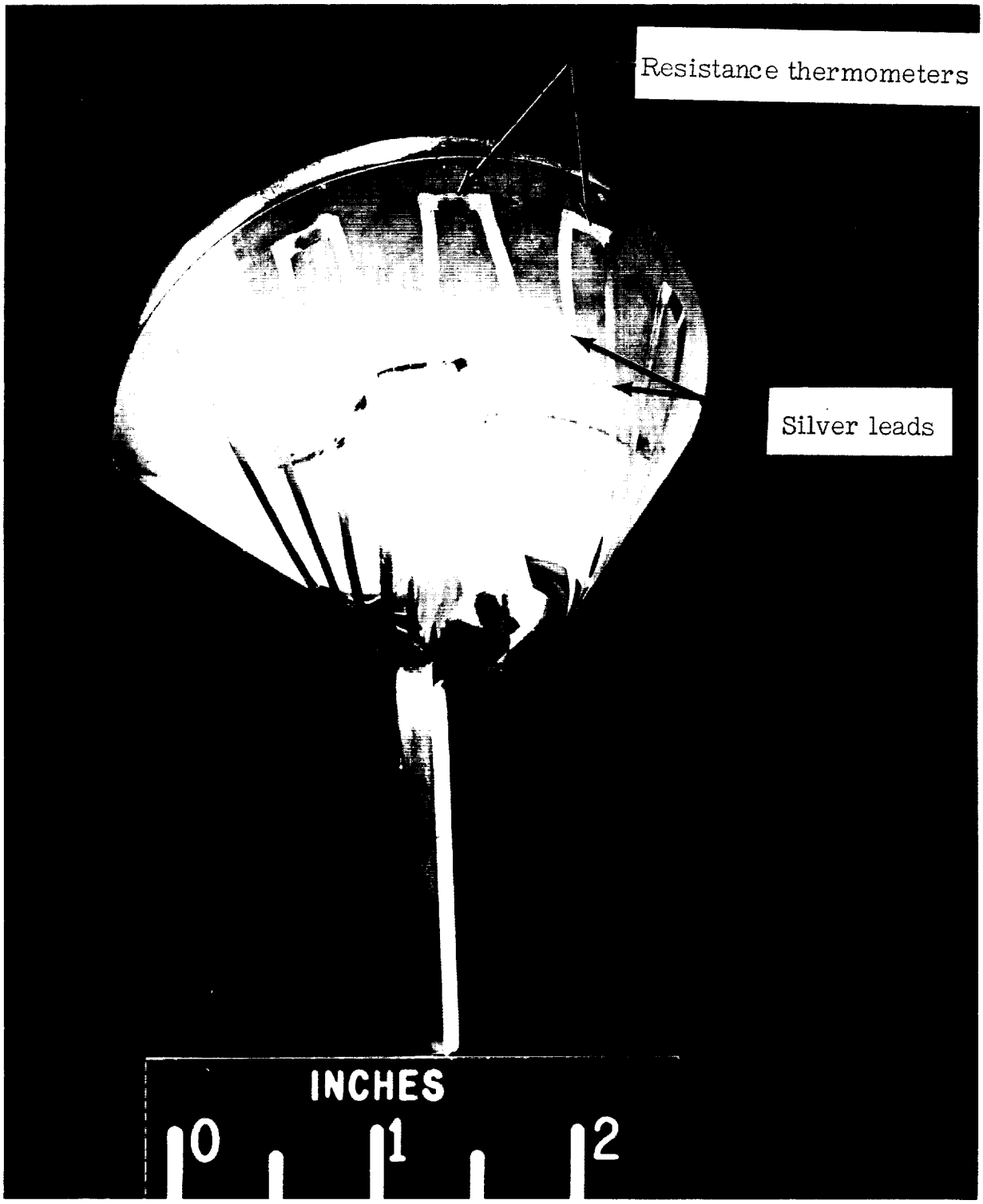

Figure 7.- Photograph of model 1. L-62-6212.1

[redacted]

[redacted]

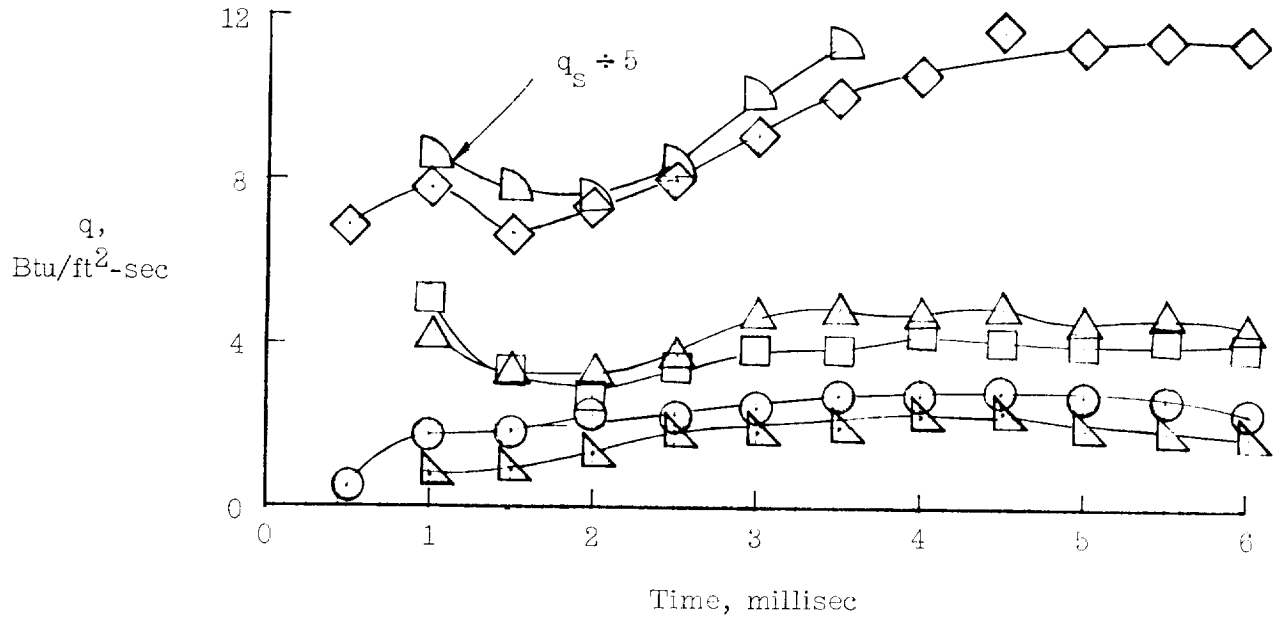

(a) Model heat-transfer rates plotted against time.

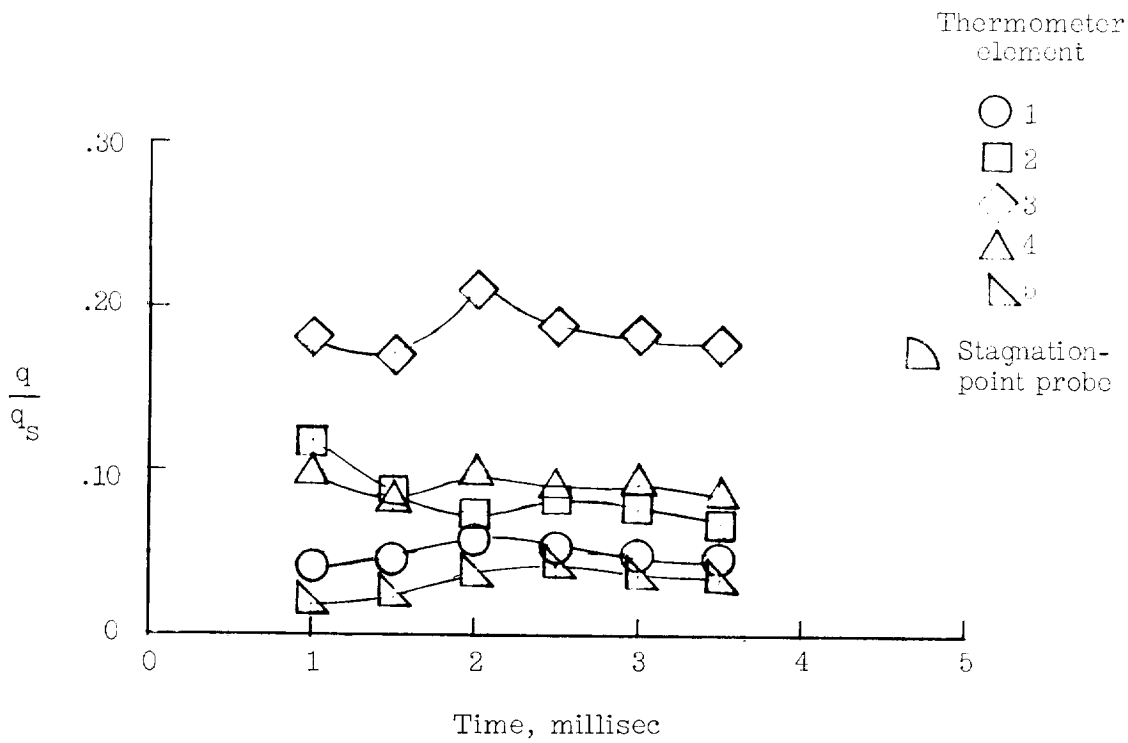

(b) Afterbody q divided by stagnation-point q plotted against time.

Figure 8.- Sample of model heat-transfer rates (run 1604).

[redacted]

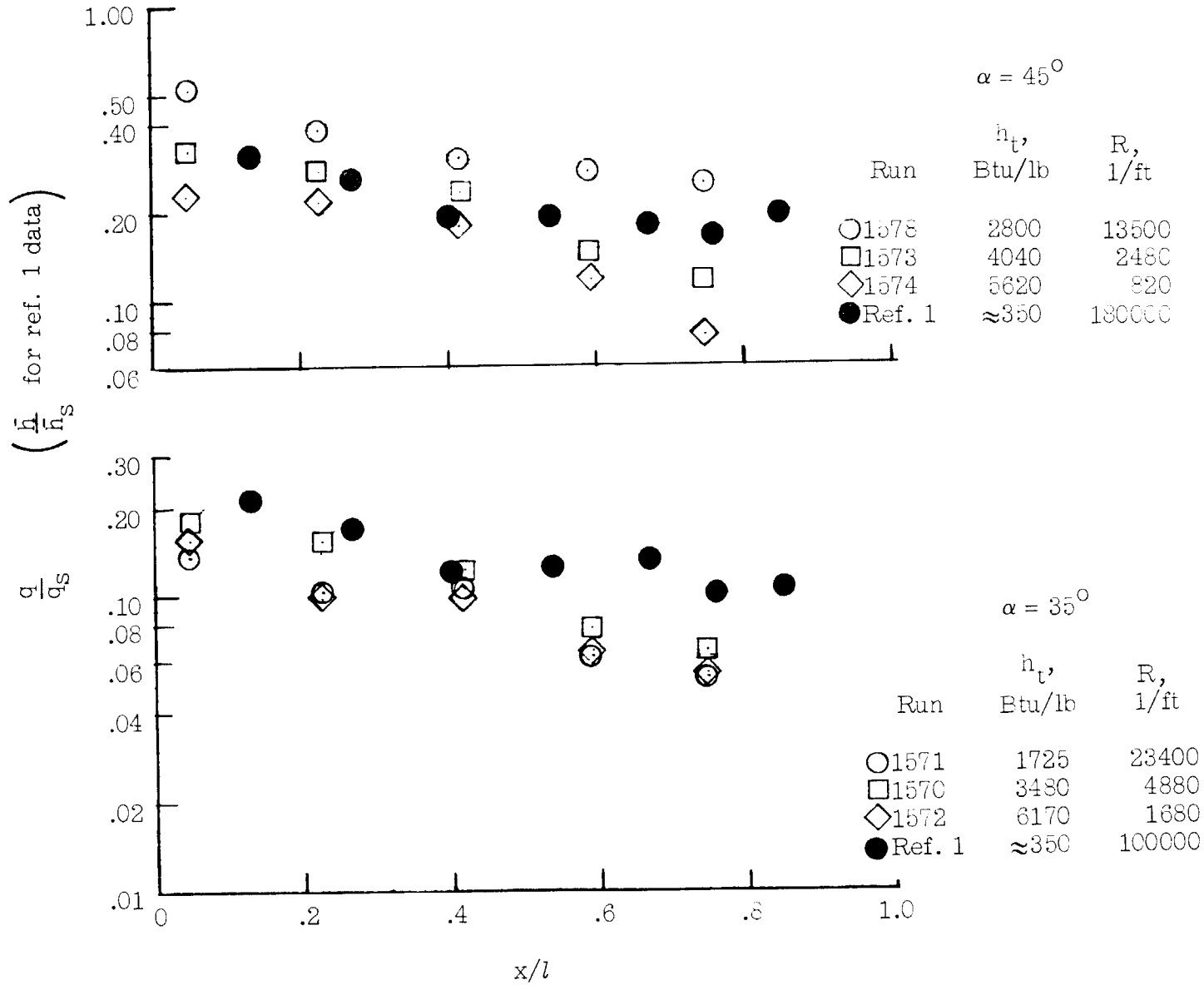

Figure 9.- Axial-distribution heat-transfer rate along $\phi = 0^\circ$ ray.

[redacted]

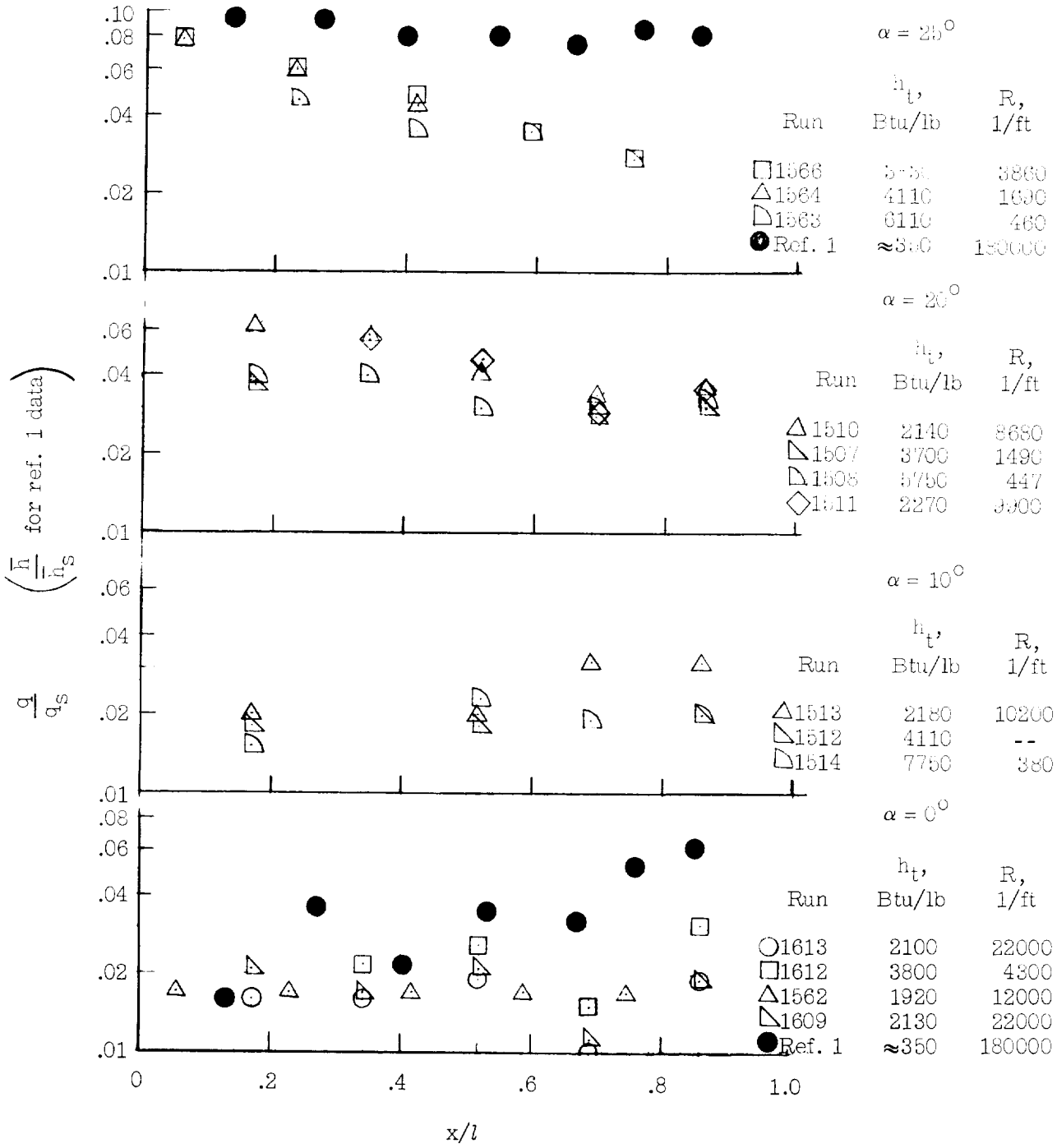

Figure 9.- Concluded.

[redacted]

[redacted]

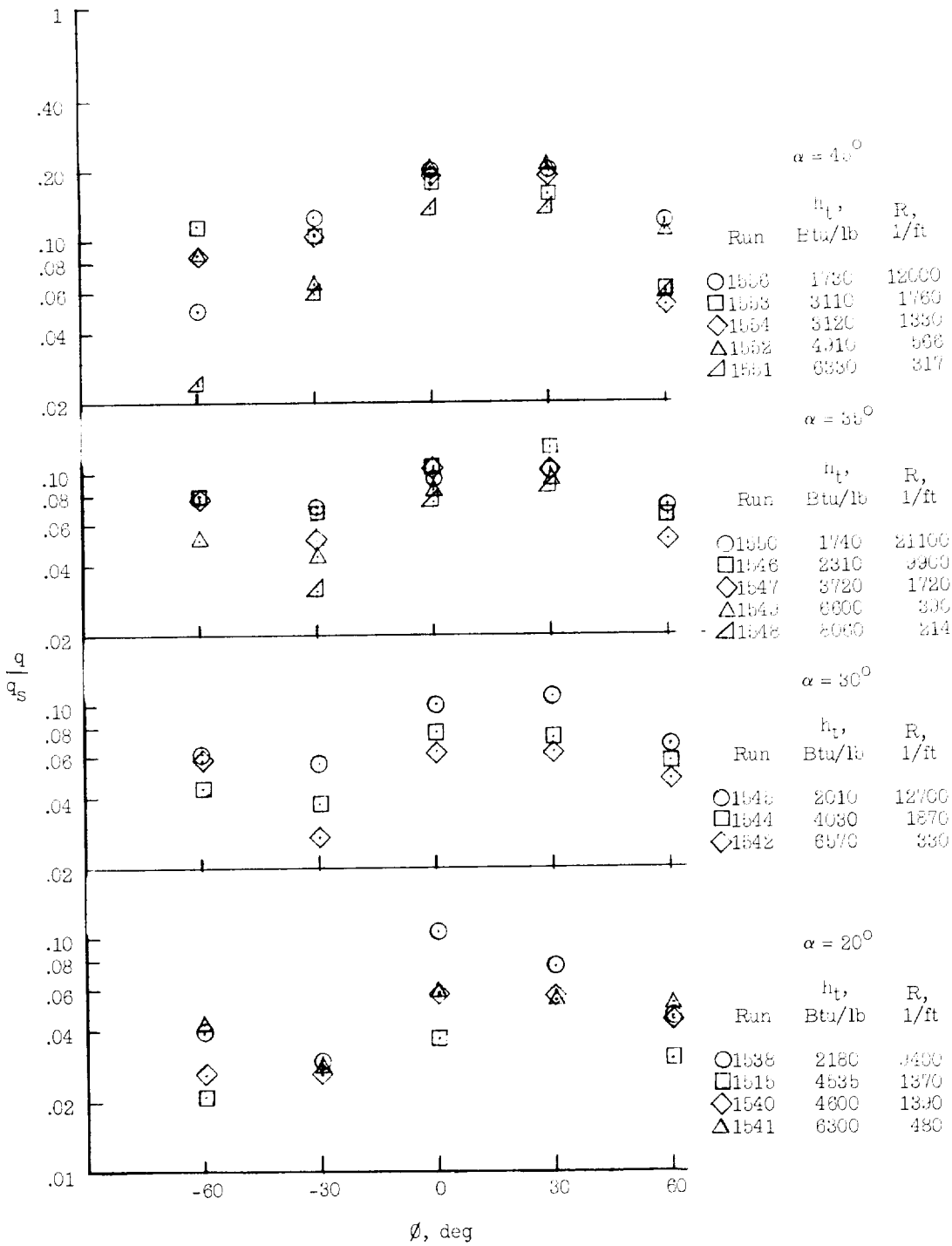

(a) Model 1 (x/l = 0.114).

Figure 10.- Lateral-distribution heat-transfer rates.

[redacted]

[redacted]

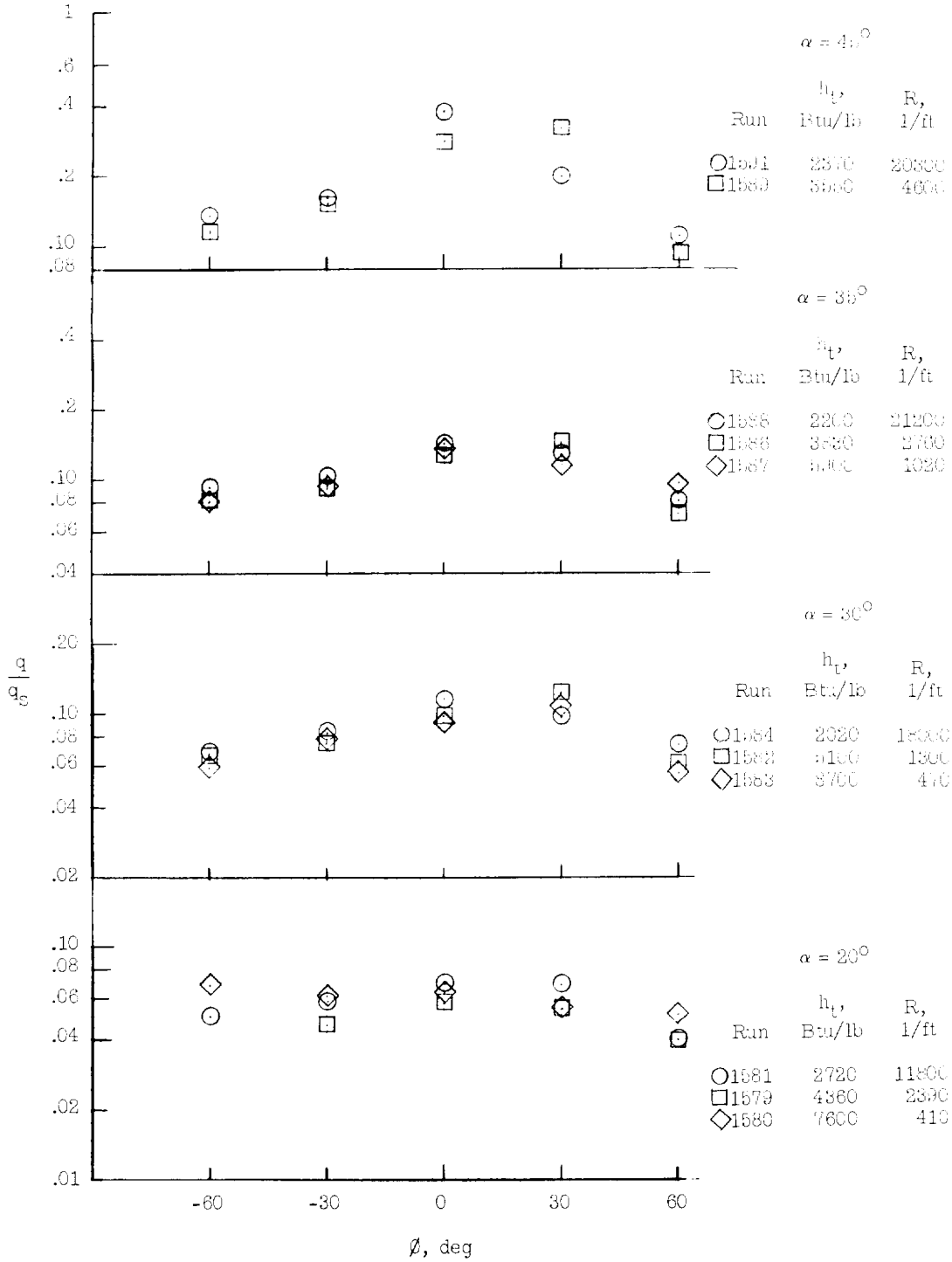

(b) Model 3 (x/l = 0.229).

Figure 10.- Continued.

[redacted]

[redacted]

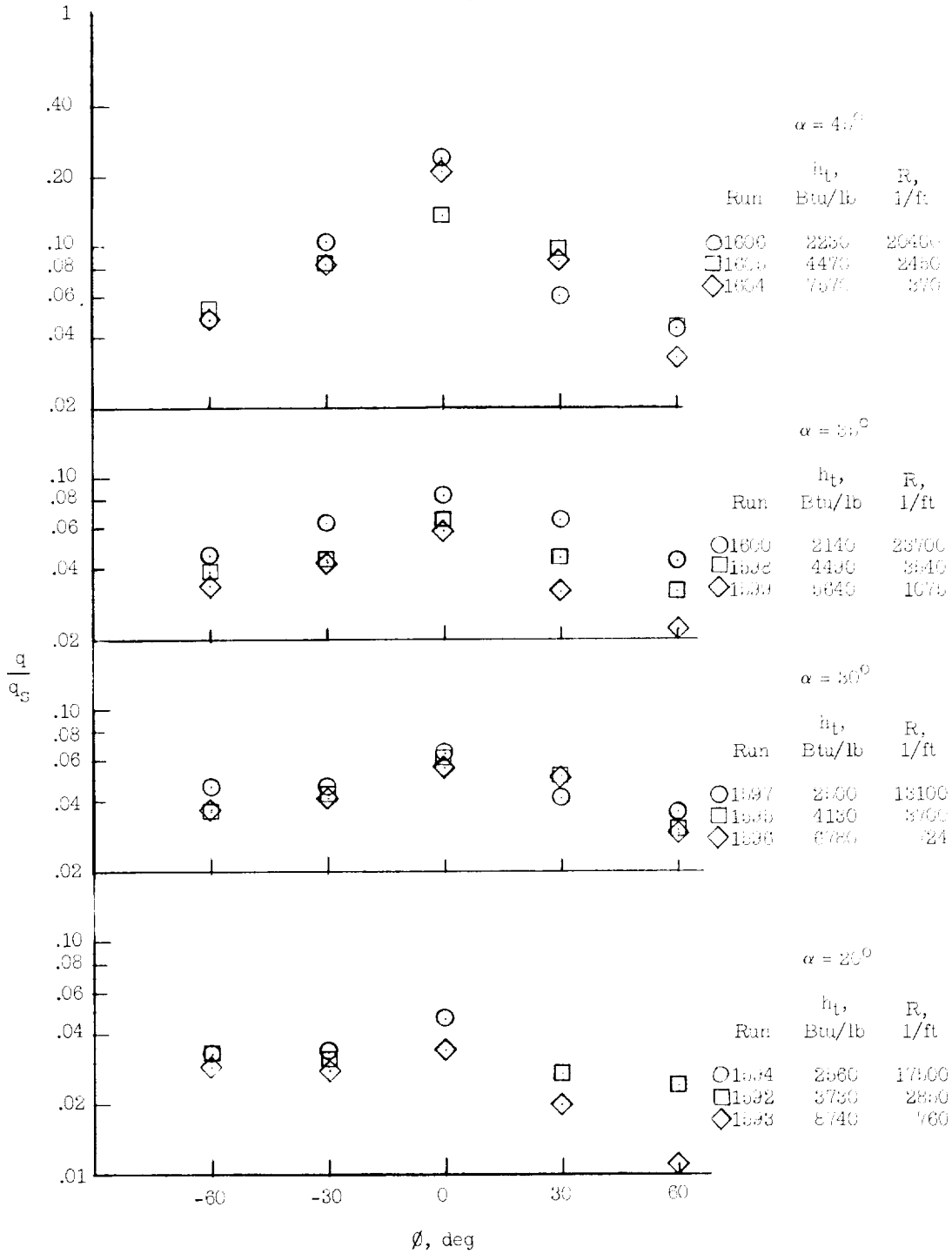

(c) Model 5 (x/l = 0.688).

Figure 10.- Concluded.

[redacted]

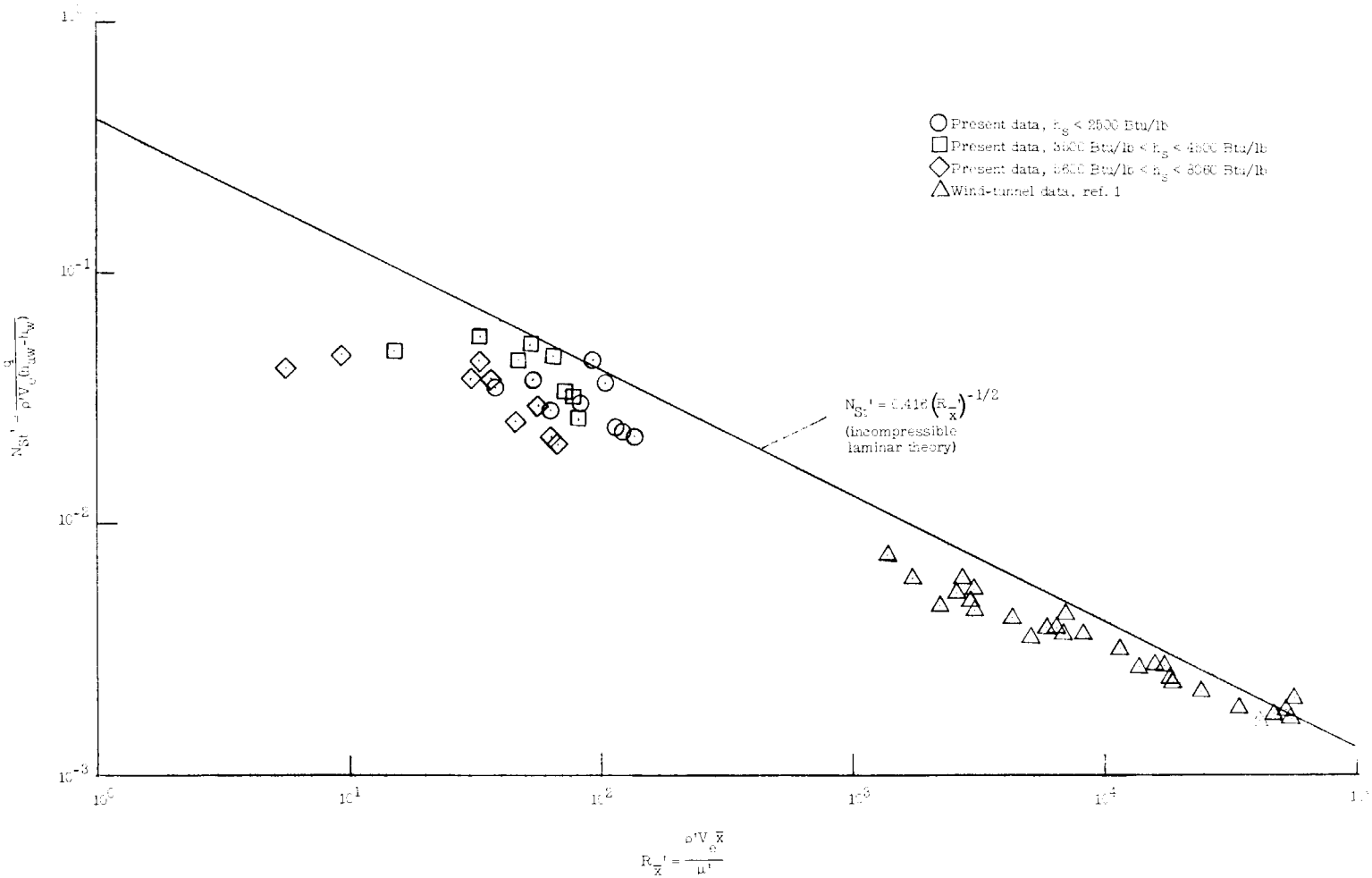

Figure 11.- Afterbody heat transfer along $\phi = 0^{\circ}$ ray at $\alpha = 35^{\circ}$ for present data and reference 1 data.

[redacted]

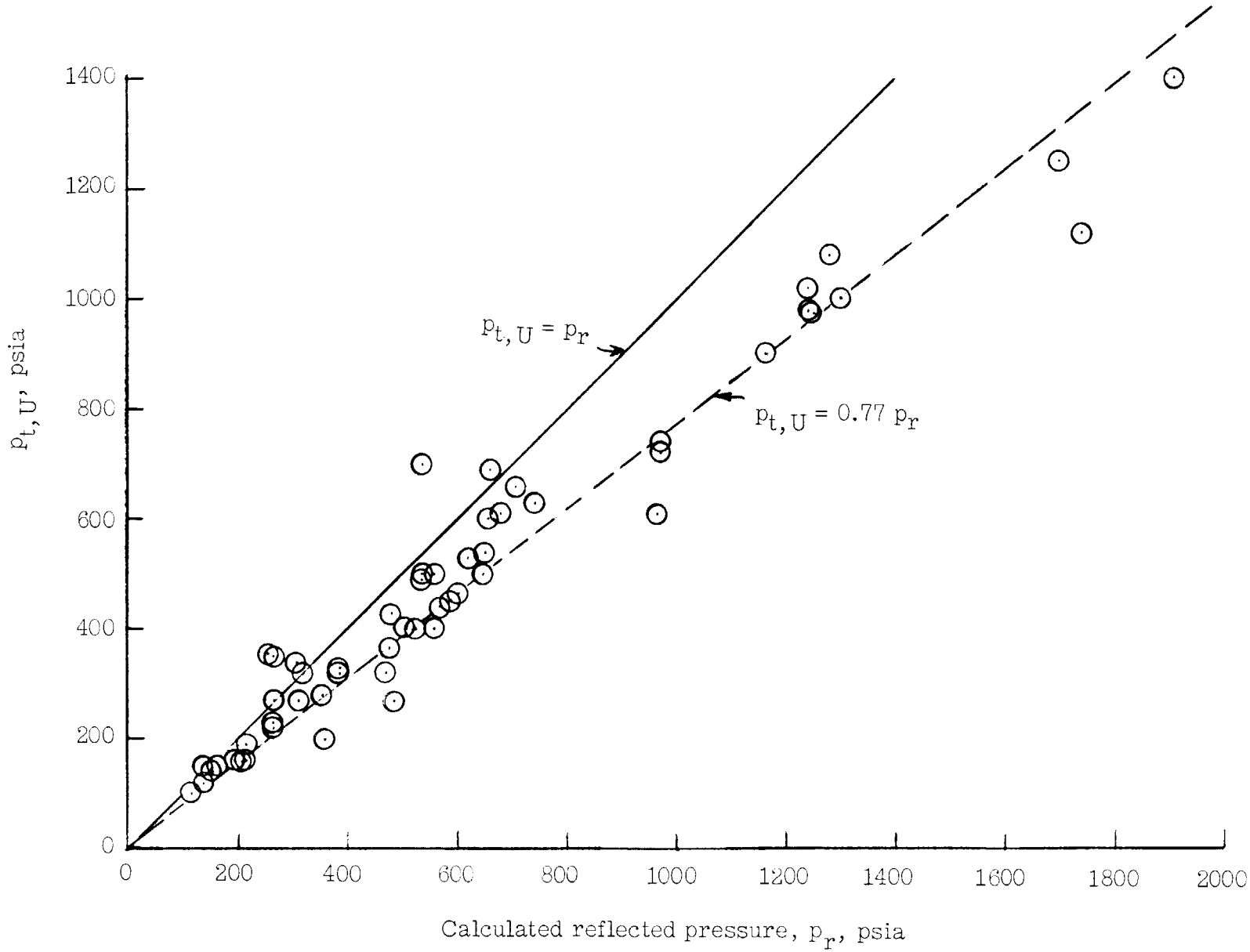

[redacted]

Figure 12.- Comparison of measured stagnation pressures with those calculated from shock Mach number.

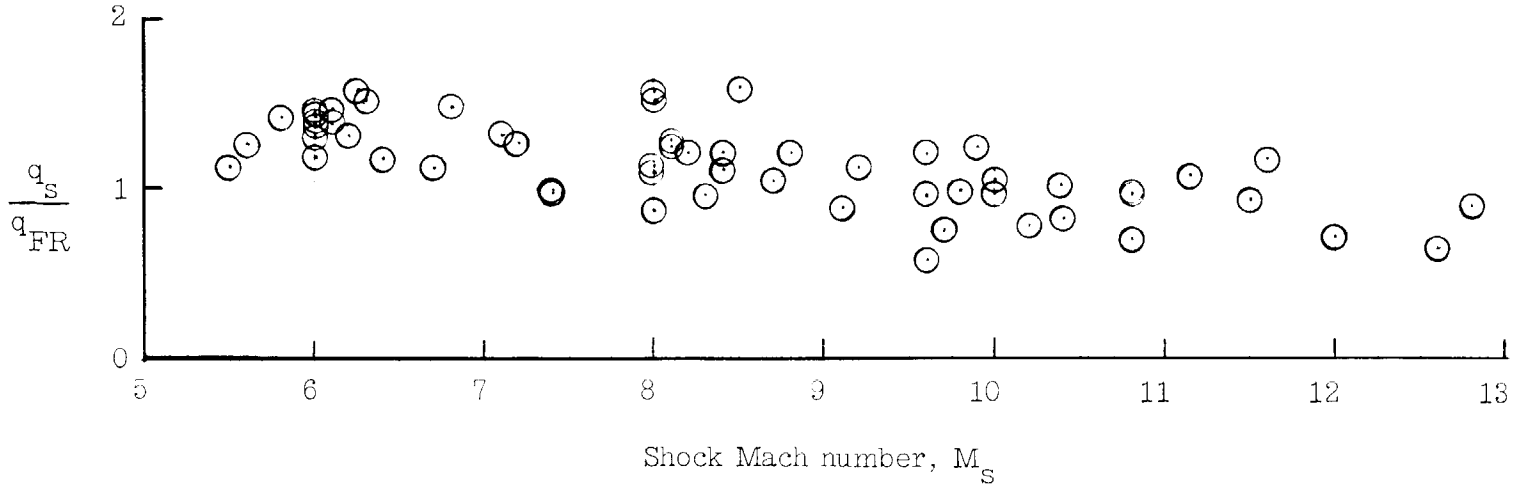

(a) Compared with theory of reference 3.

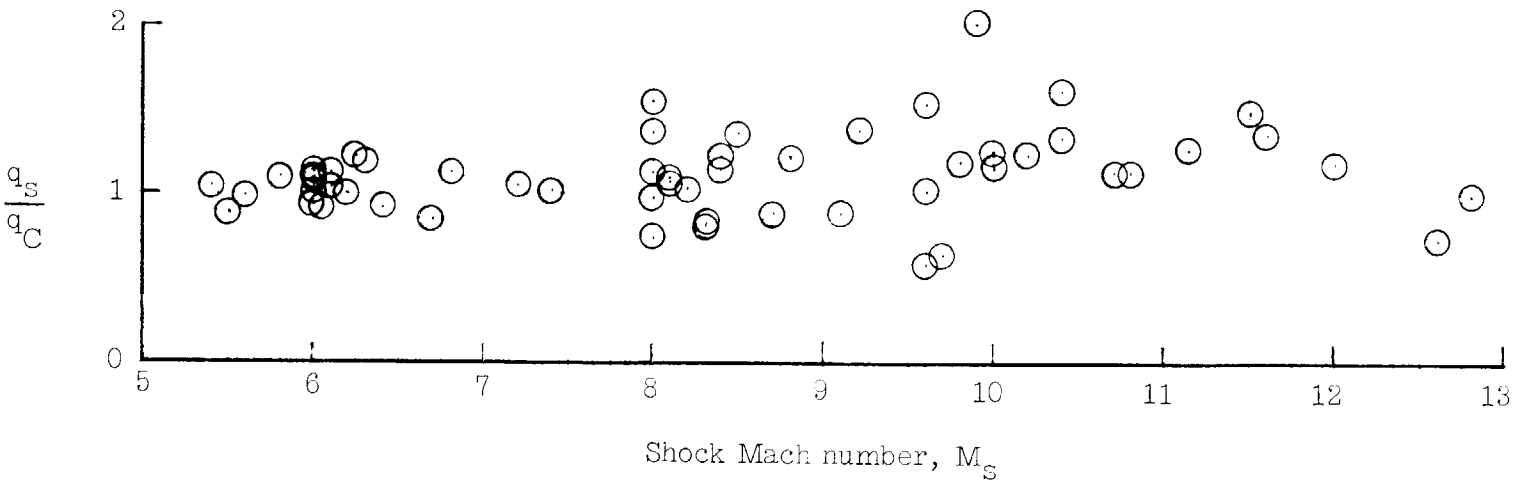

(b) Compared with theory of reference 2.

Figure 13.- Stagnation-point heat-transfer rate to sphere, compared with theories of Fay and Riddell (ref. 3) and of Cheng (ref. 2).

NASA-Langley, 1964 L-3646

NASA TM X-1042 THIS CARD UNCLASSIFIED
National Aeronautics and Space Administration.
SHOCK-TUNNEL HEAT-TRANSFER INVESTIGATION ON THE AFTERBODY OF AN APOLLO-TYPE CONFIGURATION AT ANGLES OF ATTACK UP TO 45°.
Jim J. Jones and John A. Moore. December 1964.
33p. (NASA TECHNICAL MEMORANDUM X-1042)
[redacted]

A shock-tunnel investigation of the heat transfer to the afterbody of an Apollo-type reentry configuration was made over an angle-of-attack range from 0° to 45°. The stagnation-enthalpy range covered was from 1730 to 8940 Btu/lb, the Mach number varied from 6.5 to 16.1, and the free-stream Reynolds number per foot ranged from 150 to 24000 (Reynolds number based on model diameter ranged from 58 to 6000). The results of the investigation were compared with previous results obtained in a conventional Mach 8 wind tunnel.

I. Jones, Jim J.
II. Moore, John A.
III. NASA TM X-1042

[redacted]

[redacted]

NASA

NASA TM X-1042 THIS CARD UNCLASSIFIED
National Aeronautics and Space Administration.
SHOCK-TUNNEL HEAT-TRANSFER INVESTIGATION ON THE AFTERBODY OF AN APOLLO-TYPE CONFIGURATION AT ANGLES OF ATTACK UP TO 45°.
Jim J. Jones and John A. Moore. December 1964.
33p. (NASA TECHNICAL MEMORANDUM X-1042)
[redacted]

A shock-tunnel investigation of the heat transfer to the afterbody of an Apollo-type reentry configuration was made over an angle-of-attack range from 0° to 45°. The stagnation-enthalpy range covered was from 1730 to 8940 Btu/lb, the Mach number varied from 6.5 to 16.1, and the free-stream Reynolds number per foot ranged from 150 to 24000 (Reynolds number based on model diameter ranged from 58 to 6000). The results of the investigation were compared with previous results obtained in a conventional Mach 8 wind tunnel.

I. Jones, Jim J.
II. Moore, John A.
III. NASA TM X-1042

[redacted]

THIS CARD UNCLASSIFIED

NASA

NASA TM X-1042 THIS CARD UNCLASSIFIED
National Aeronautics and Space Administration.
SHOCK-TUNNEL HEAT-TRANSFER INVESTIGATION ON THE AFTERBODY OF AN APOLLO-TYPE CONFIGURATION AT ANGLES OF ATTACK UP TO 45°.
Jim J. Jones and John A. Moore. December 1964.
33p. (NASA TECHNICAL MEMORANDUM X-1042)
[redacted]

A shock-tunnel investigation of the heat transfer to the afterbody of an Apollo-type reentry configuration was made over an angle-of-attack range from 0° to 45°. The stagnation-enthalpy range covered was from 1730 to 8940 Btu/lb, the Mach number varied from 6.5 to 16.1, and the free-stream Reynolds number per foot ranged from 150 to 24000 (Reynolds number based on model diameter ranged from 58 to 6000). The results of the investigation were compared with previous results obtained in a conventional Mach 8 wind tunnel.

I. Jones, Jim J.
II. Moore, John A.
III. NASA TM X-1042

[redacted]

THIS CARD UNCLASSIFIED

NASA

NASA TM X-1042 THIS CARD UNCLASSIFIED
National Aeronautics and Space Administration.
SHOCK-TUNNEL HEAT-TRANSFER INVESTIGATION ON THE AFTERBODY OF AN APOLLO-TYPE CONFIGURATION AT ANGLES OF ATTACK UP TO 45°.
Jim J. Jones and John A. Moore. December 1964.
33p. (NASA TECHNICAL MEMORANDUM X-1042)
[redacted]

A shock-tunnel investigation of the heat transfer to the afterbody of an Apollo-type reentry configuration was made over an angle-of-attack range from 0° to 45°. The stagnation-enthalpy range covered was from 1730 to 8940 Btu/lb, the Mach number varied from 6.5 to 16.1, and the free-stream Reynolds number per foot ranged from 150 to 24000 (Reynolds number based on model diameter ranged from 58 to 6000). The results of the investigation were compared with previous results obtained in a conventional Mach 8 wind tunnel.

I. Jones, Jim J.
II. Moore, John A.
III. NASA TM X-1042

[redacted]

[redacted]

NASA

[redacted]

"The aeronautical and space activities of the United States shall be conducted so as to contribute . . . to the expansion of human knowledge of phenomena in the atmosphere and space. The Administration shall provide for the widest practicable and appropriate dissemination of information concerning its activities and the results thereof."

—NATIONAL AERONAUTICS AND SPACE ACT OF 1958

NASA SCIENTIFIC AND TECHNICAL PUBLICATIONS

TECHNICAL REPORTS: Scientific and technical information considered important, complete, and a lasting contribution to existing knowledge.

TECHNICAL NOTES: Information less broad in scope but nevertheless of importance as a contribution to existing knowledge.

TECHNICAL MEMORANDUMS: Information receiving limited distribution because of preliminary data, security classification, or other reasons.

CONTRACTOR REPORTS: Technical information generated in connection with a NASA contract or grant and released under NASA auspices.

TECHNICAL TRANSLATIONS: Information published in a foreign language considered to merit NASA distribution in English.

TECHNICAL REPRINTS: Information derived from NASA activities and initially published in the form of journal articles.

SPECIAL PUBLICATIONS: Information derived from or of value to NASA activities but not necessarily reporting the results of individual NASA-programmed scientific efforts. Publications include conference proceedings, monographs, data compilations, handbooks, sourcebooks, and special bibliographies.

Details on the availability of these publications may be obtained from:

SCIENTIFIC AND TECHNICAL INFORMATION DIVISION

NATIONAL AERONAUTICS AND SPACE ADMINISTRATION

Washington, D.C. 20546

[redacted]